

**University of São Paulo  
“Luiz de Queiroz” College of Agriculture**

**Remote sensing application in forest monitoring and climate changes**

**Léo Eiti Haneda**

Dissertation presented to obtain the degree of Master in  
Science. Area: Forest Resources. Option in:  
Conservation of Natural Ecosystems

**Piracicaba  
2023**

**Léo Eiti Haneda**  
**Forestry Engineer**

**Remote sensing application in forest monitoring and climate changes**

versão revisada de acordo com a Resolução CoPGr 6018 de 2011

Advisor:

Prof. Dr. **PEDRO HENRIQUE SANTIN BRANCALION**

Dissertation presented to obtain the degree of Master in  
Science. Area: Forest Resources. Option in:  
Conservation of Natural Ecosystems

**Piracicaba**  
**2023**

**Dados Internacionais de Catalogação na Publicação  
DIVISÃO DE BIBLIOTECA – DIBD/ESALQ/USP**

Haneda, Léo Eiti

Remote sensing application in forest monitoring and climate changes /  
Léo Eiti Haneda - - versão revisada de acordo com a Resolução CoPGr  
6018 de 2011. - - Piracicaba, 2023

66 p.

Dissertação (Mestrado) - - USP / Escola Superior de Agricultura "Luiz  
de Queiroz".

1. Multispectral orbital images 2. Forest types 3. LiDAR 4. Forest  
degradation I. Remote sensing application in forest monitoring and climate  
changes

## ACKNOWLEDGEMENTS

Firstly, I would like to express my gratitude to my family for their love, care, trust, and unconditional support. There are not enough words to describe my eternal love and gratitude, I dedicate all my achievements to you.

To my brothers from my baseball team "Nippon Blue Jays," who have been by my side since I can remember and are part of my roots.

To República Antro and all its residents, for being part of the most important time of my life, a place of many life experiences and self-discovery.

To my advisor Pedro Brancalion for his support and trust. And, most importantly, to my advisor and “camarada” Danilo Almeida for all the support, trust, advice, friendship, and encouragement.

To CAPES for the financial support, who granted me with a scholarship in my first year of the master's program. And to BrCarbon and my coworkers, for the opportunities, learning experiences, and friendships in this short period of time.

## CONTENTS

<b>RESUMO</b> .....		<b>6</b>
<b>ABSTRACT</b> .....		<b>7</b>
<b>1. INTRODUCTION</b> .....		<b>9</b>
<b>2. FOREST LANDSCAPE RESTORATION: SPECTRAL BEHAVIOR AND DIVERSITY OF TROPICAL TREE COVER CLASSES</b> .....		<b>11</b>
Abstract	11	
2.1. Introduction .....		11
2.2. Material and Methods .....		13
2.2.1. <i>Study area and tree cover classes</i> .....		13
2.2.2. <i>Satellite images</i> .....		17
2.2.3. <i>Model attributes</i> .....		17
2.2.4. <i>Data analysis</i> .....		21
2.2.5. <i>Thematic map</i> .....		22
2.3. Results.....		22
2.3.1. <i>Tree cover classes characterization</i> .....		22
2.3.2. <i>Tree cover classes classification</i> .....		26
2.4. Discussion .....		31
References	35	
Supplementary Material .....		39
<b>3. SECOND`D` OF REDD+ PROJECTS: APPLICATIONS OF UAV-LIDAR ON LOCAL DEGRADATION MONITORING</b> .....		<b>43</b>
<b>ABSTRACT</b> .....		<b>43</b>
3.1. Introduction .....		43
3.2. Material and Methods .....		47
3.2.1. <i>Study Area</i> .....		47
3.2.2. <i>LiDAR Data</i> .....		48
3.2.3. <i>Statistical Modelling</i> .....		48
3.3. Results.....		50
3.3.1. <i>Statistical modelling</i> .....		50
3.4. Discussion .....		52
3.5. Conclusion .....		56
References	57	
Supplementary Material .....		61
<b>4. GENERAL CONCLUSION</b> .....	ERROR! BOOKMARK NOT DEFINED.	



## RESUMO

### **Aplicações do sensoriamento remoto no monitoramento florestal e mitigação das mudanças climáticas**

Nos últimos anos, as tecnologias de sensoriamento remoto têm experimentado avanços significativos, impulsionados pela introdução de novos sensores e técnicas avançadas de processamento de dados. Esses avanços têm permitido uma observação das florestas de maneiras antes inacessíveis. Com isso, surgem grandes expectativas em relação a essas tecnologias no enfrentamento dos desafios impostos pelas mudanças climáticas. Esta dissertação consiste em dois capítulos, sendo o primeiro focado no uso de imagens orbitais multiespectrais de alta resolução e técnicas avançadas de manipulação de dados para o monitoramento e classificação de diferentes tipos de cobertura florestal. O objetivo é fornecer suporte a programas de restauração florestal em paisagens. O segundo capítulo aborda a utilização de dados LiDAR para o monitoramento local da degradação em projetos REDD+, visando investigar as aplicações dessa tecnologia na conservação e monitoramento florestal. Nossos resultados evidenciaram o grande potencial das tecnologias de sensoriamento remoto para abordar questões relacionadas à mitigação das mudanças climáticas, tanto em termos de restauração quanto de conservação florestal. No entanto, é necessário realizar trabalhos subsequentes para desenvolver metodologias robustas e replicáveis, a fim de permitir que as tecnologias de sensoriamento remoto desempenhem um papel fundamental na superação dos desafios impostos pelas mudanças climáticas.

Palavras-chave: Imagem orbital multiespectral, Tipologias florestais, LiDAR, Degradação florestal

## ABSTRACT

### **Remote sensing application in forest monitoring and climate changes**

Remote sensing technologies have made significant advancements in recent decades, with the introduction of new sensors and data manipulation techniques that allow us to observe forests in previously inaccessible ways. With these advancements, there are high expectations for these technologies to address the challenges posed by climate change. This master's thesis consists of two chapters, one using a passive sensor and the other using an active sensor. The first chapter investigates the potential of high-resolution multispectral satellite imagery and different data manipulation techniques for monitoring forest landscapes and classifying different forest types, with the aim of supporting landscape forest restoration programs. The second chapter focuses on the use of LiDAR data for monitoring degradation in REDD+ projects at a local level, aiming to explore the applications of this technology in forest monitoring and conservation. Our results have shown the great potential of remote sensing technologies in addressing various issues related to climate change mitigation, both for forest restoration and conservation. However, further work needs to be done to develop robust and replicable methodologies that allow remote sensing technologies to play a key role in overcoming the significant challenges posed by climate change.

Keywords: Multispectral orbital images, Forest types, LiDAR, Forest degradation





## 1. INTRODUCTION

This master's dissertation aims to evaluate the potential of different remote sensing techniques for forest monitoring, focusing on methodologies that can be applied to real-world problems. Remote sensing technologies have made significant advancements in recent decades, with the introduction of new sensors and data manipulation techniques that allow us to observe forests in previously inaccessible ways. With these advancements, there are high expectations for these technologies to address the challenges related to forest restoration and conservation. Therefore, continuous development of research is necessary to fully harness their potential and create new methodologies to reduce their impacts.

Previously, forest monitoring relied mostly on field assessments to evaluate forest characteristics and conditions. But this process is usually high costly and time-consuming, which makes the monitoring of extensive landscapes ineffective. Remote sensing technologies have the potential to improve forest monitoring in all sorts of levels. The use of satellite imagery enhances the forest monitoring in a landscape levels, as it allows the observation of thousands of hectares. Furthermore, the high spatial and spectral resolution satellite images allow complex forest studies, for example, the distinction of different types of forests. On the other side, the use of active sensors on board UAV's (e.g., LiDAR sensor) allow the characterization of the forest structure in a more detailed way, which allows the identification of disturbance in a local level.

This master's dissertation consists of two chapters focused on the use of remote sensing for forest monitoring. The first chapter involves the already published scientific article titled "Forest Landscape Restoration: Spectral behavior and diversity of tropical tree cover classes". This work utilizes high-resolution (5-meter) multispectral satellite images from the VEN $\mu$ S satellite, along with different geospatial data manipulation techniques and the Random Forest machine learning algorithm, to perform supervised classification of different forest typologies commonly found in landscape restoration programs. Locating and understanding the distribution of different forest typologies in the landscape is the first step in assessing and quantifying biodiversity and ecosystem services. Once these typologies are mapped, subsequent approaches such as field surveys and LiDAR flights can be conducted to verify their benefits for nature and people, enhancing the scale and efficiency of forest landscape restoration efforts.

The second chapter is titled "Second 'D' of REDD+ Projects: Applications of UAV-LiDAR for local degradation monitoring." The objective of this second work was to evaluate the use of LiDAR data for local monitoring of forest degradation in REDD+ projects and

assess its impact on forest structure. Forest degradation, due to its challenging detection, often receives limited attention in forest monitoring programs. LiDAR technology has great potential to fill this gap by enabling detailed characterization of the forest and identification of structural changes. However, as a relatively new technology, REDD+ projects lack an established methodology by the certifying body for the use of LiDAR data in local degradation monitoring. Hence, this work aims to develop a methodology for assessing the degree of local degradation in forests within REDD+ projects. We employed a statistical modeling approach to relate forest structural characteristics with the distance from potential degradation sources (anthropized areas). Our results showed how forest structure is impacted by adjacent opened areas, and that the edge effect infiltrated only the first 50 meters of the forests, suggesting a high level of conservation within the REDD+ project areas.

## 2. FOREST LANDSCAPE RESTORATION: SPECTRAL BEHAVIOR AND DIVERSITY OF TROPICAL TREE COVER CLASSES

### Abstract

Forest landscape restoration (FLR) commitments have been established in the past years to restore over 200 million hectares, mostly through the implementation of several different restorative practices in degraded lands, ranging from commercial tree monocultures to restoration plantings. The potential of such contrasting restorative practices to support biodiversity conservation and ecosystem services provision vary greatly over space and time, making the monitoring of FLR programs an emerging challenge. Remote sensing techniques, together with new technologies for data acquisition, treatment, and analysis have proven to be strategic for planning and monitoring FLR, yet there are still important unresolved questions. Here, we evaluated the potential of multispectral orbital images of the high spatial and spectral resolution VEN $\mu$ S sensor to classify the spectral behavior and diversity of tree cover classes commonly found in FLR programs. We assessed how six tree cover classes (savanna woodlands, old- and second-growth semi-deciduous forests, young restoration plantings, and eucalyptus and pine tree monocultures) located in a study landscape in southeastern Brazil differ according to their spectral response (winter and summer bands, and vegetation indices), canopy variability (textural features), seasonal behavior (delta layers - difference between summer and winter vegetation indexes), and spectral diversity. We used the Random Forest algorithm to generate the models and evaluate how the tree cover classes differ in the classification and how the metrics performed. We achieved high values of global accuracy (91.9%) and “F1 score” (above 0.8) for all tree cover classes, in which second-growth forest presented the lowest accuracy. The textural layers, delta layers, and the spectral diversity layers were the most important attributes to discriminate among tree cover classes. We demonstrate here the potential of using VEN $\mu$ S or similar sensor images together with different image processing and machine learning algorithms to monitor FLR programs and advance with the qualification of tree cover gains resulting from these initiatives.

### Keywords

Remote sensing, forest restoration, tropical forest, forest types, multispectral images, high resolution, random forest

### 2.1. Introduction

Forest landscape restoration (FLR) has been promoted at an unprecedented scale, with more than 60 nations pledging the recovery of ecological functionality of over 200 million hectares of degraded and deforested landscapes as part of the Bonn Challenge. Different tree cover restoration approaches have been adopted in FLR programs, including mixed native species plantations, assisted natural regeneration, agroforestry, and commercial tree monocultures, which vary greatly in species composition, structure, and functionality (Lamb,

2018; Stanturf et al., 2019; Temperton et al., 2019). The proportion of each of these approaches in FLR programs has been widely debated - and criticized -, as a large share of the commitments have been based on large-scale monocultures of exotic trees (Lewis et al., 2019), which provides lower levels of ecological benefits than native forests (Hua et al., 2022). Thus, FLR benefits to people and nature will heavily rely on the “blend” of restoration approaches used in each program, being the monitoring of the diversity, structure and dynamics of different tree cover classes over space and time, an emerging challenge for research. The complex, heterogeneous landscapes to be established by FLR programs makes monitoring difficult. Restoration monitoring has been mostly done through field surveys (Chaves et al., 2015; Wortley et al., 2013), making it costly, time consuming and, in many cases, operationally infeasible. In this regard, remote sensing techniques together with new technologies for collecting, processing, and analyzing images has proved to be a strategic tool for planning and monitoring FLR, allowing the analysis of previously inaccessible information and enabling more in-depth and broad-scale assessments (Almeida et al., 2020; Houet et al., 2010), yet there are still important unresolved questions regarding the distinction of different tree cover classes.

Multispectral orbital sensors with high spatial and spectral resolution allow accessing more detailed information about the land cover, indicating how each target behaves concerning the reflectance of electromagnetic radiation. The multispectral images of the VEN $\mu$ S satellite sensor are a good example of new data acquisition technology, providing data with high spatial (5 meters), temporal (2 days), and spectral (12 bands) resolution. The VEN $\mu$ S spectral bands includes narrow bands located in the “red-edge” region (4 bands from 667 to 782 nm) that allow further studies on vegetation, as this is the region of the electromagnetic spectrum where measured reflectance is more sensitive to photosynthetic chlorophyll pigments (Herscovitz and Barnett, 2007). Simultaneously, technological progress with data storage and processing makes it possible to manipulate large volumes of information, enabling more robust and complex analyses. Image processing techniques allow computing a variety of variables that can be used to improve tree cover class classification, such as texture metrics that indicate the variation of pixel values along the surface and multitemporal data computation that helps the characterization of forests through their seasonal phenology (Kim et al., 2009; Tottrup, 2004; Zhu and Liu, 2014). Machine learning algorithms have also proved to be a useful tool for different types of study, the Random Forest' algorithm stands out for its high accuracy, fast processing, and applicability to data from geographic information systems, as it is one of the most popular algorithms used for

works in this area (Belgiu and Drăguț, 2016; Gislason et al., 2006). All these factors combined contribute to make satellite remote sensing a powerful tool for forest monitoring and landscape restoration, but more studies must be carried out to explore the full potential of the method.

Here, we evaluated the potential of multispectral orbital images of the high spatial and spectral resolution VENμS sensor to classify the spectral behavior and diversity of tree cover classes commonly found in FLR programs. We employed novel analytical approaches based on the use of images collected at different seasons of the year and image processing algorithms that enhance the spectral diversity of tree cover classes, going beyond the traditional focus on static spectral characteristics. More specifically, we (i) characterized tree cover classes based on spectral diversity and behavior, (ii) evaluated the classification of tree cover classes using the Random Forest algorithm, (iii) evaluate the effect of adding textural and spectral diversity metrics to the model's accuracy, and (iv) generated a thematic map of tree cover classes for the entire forest landscape under study.

## 2.2. Material and Methods

### 2.2.1. Study area and tree cover classes

We conducted the study at the Itatinga Experimental Station of Forest Sciences (48°38' S, 23°2' W; Itatinga-SP, southeastern Brazil), of the University of São Paulo (Figure 1). Over the last 15 years, the annual mean precipitation was 1,360 mm and the average temperature was 19.3°C (Battie-Laclau et al., 2014). The station (2,170 hectares) is located in a transition area between the Cerrado (Brazilian savanna) and Atlantic Forest phytogeographic domains, with native ecosystems comprised of seasonal semideciduous forests, riparian forests, and savannas (de Oliveira Santos et al., 2019). The station is covered by a very heterogeneous mosaic of tree cover classes, resulting from decades of development of new genetic materials and technology for commercial forestry and new approaches for restoring native ecosystems. The studied region also contains large areas of monocultures of different species of *Eucalyptus* sp. (*E. grandis*, *E. urograndis*, *E. robusta*, *E. urophylla*, *E. dunnii*, *E. cloeziana*, and hybrids, among others), pine trees (*P. elliottii*, *P. taeda*, *P. tecunumanii*, among others), and other exotic species (Figure 1).

We selected the main tree cover classes found at the station, based on the composition, structure, and management purpose of the ecosystems: “Eucalyptus monoculture” (EucaMono), “Pine trees monoculture” (PineMono), “Old-growth semidecidual forest” (OGFor), “Second-growth semidecidual forest” (SGFor), “Second-growth savanna woodland”

(SGSav), “Young restoration planting” (YRest) and “Bare soil” (BSoil) (Table 1). Polygons (hereafter “sampling polygons”) were delimited within each tree cover class, using an existing land use map available for the station and confirmed with *in situ* visits.

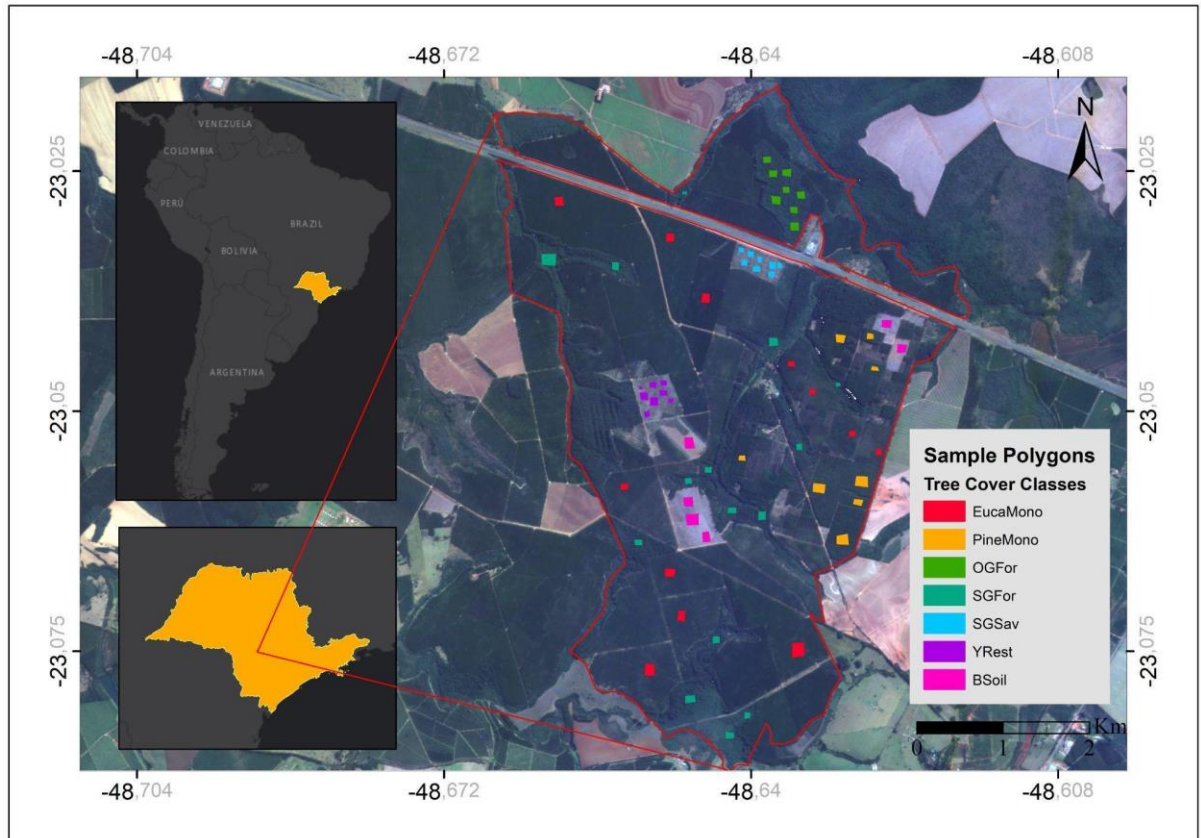











Figure 1. Location of the Itatinga Experimental Station-SP, with the sample polygons of each tree cover class used to generate the classification model, on a colored composition (R = B7, G = B4, B = B2) of the image VENμS on August 17, 2019. Classes are: “Eucalyptus monoculture” (EucaMono), “Pine trees monoculture” (PineMono), “Old-growth semidecidual forest” (OGFor), “Second-growth semidecidual forest” (SGFor), “Second-growth savanna woodland” (SGSav), “Young restoration planting” (YRest) and “Bare soil” (BSoil).

Table 1. Description of the tree cover classes included in the study: structural characteristics, and illustrative pictures with capture angles of 0°, 45°, and 90°.

Tree Cover Classes	Description	0°	45°	90°
<i>Eucalyptus monoculture</i> ("EucaMono")	<ul style="list-style-type: none"> <li>- Monocultural plantations of several <i>Eucalyptus</i> sp.</li> <li>- 2-20 years old</li> <li>- Broadleaved trees</li> <li>- Tall trees</li> <li>- Closed canopy</li> <li>- Absence of native species regeneration in the understory</li> <li>- High density of individuals</li> <li>- Low species diversity</li> </ul>			
<i>Pine trees monoculture</i> ("PineMono")	<ul style="list-style-type: none"> <li>- Monocultural plantations of several <i>Pinus</i> sp.</li> <li>- 20-30 years old</li> <li>- Needled trees</li> <li>- Tall trees</li> <li>- Closed canopy</li> <li>- Absence of native species regeneration in the understory</li> <li>- High density of individuals</li> <li>- Low species diversity</li> </ul>			
<i>Old-growth semidecidual forest</i> ("OGFor")	<ul style="list-style-type: none"> <li>- Remaining conserved forest</li> <li>- +80 years old</li> <li>- Broadleaved trees</li> <li>- Tall trees</li> <li>- Closed canopy</li> <li>- Dense understory of native</li> </ul>			



species

- High density of individuals
- High species diversity

*Second-growth semideciduous forest*  
 (“SGFor”)

- Secondary forests established by spontaneous regeneration
- ~50 years old
- Broadleaved trees
- Tall trees
- Closed canopy
- Presence of understory
- High density of individuals
- High species diversity



*Second-growth savanna woodland*  
 (“SGSav”)

- Native vegetation established from natural regeneration
- ~25 years old
- Broadleaved trees
- Small trees
- Open canopy
- Low density of individuals
- High species diversity



*Young restoration planting*  
 (“YRest”)

- Restoration plantings established through nucleation approach
- ~2 years old
- Broadleaved trees
- Small trees
- Open canopy
- High species diversity



*Bare soil*  
 (“BSoil”)

- Bare ground areas

-

-

-

### 2.2.2. Satellite images

In this study, we used VEN $\mu$ S satellite images. The VEN $\mu$ S mission is a product of the partnership between the Israel Space Agency and the CNES (French Space Agency) and has the main goal of providing data to support scientific studies related to the analysis, monitoring, and modeling of land cover dynamics, helping in monitoring natural resources and climate change mitigation. Four of the bands are found in the “red edge” region, located in the transition zone between the visible and near infrared spectrum, where leaf reflectance is sensitive to photosynthetic pigments (Dedieu et al. al., 2006; Herscovitz and Barnett, 2007). Of special interest are two narrow bands centered at 742 and 782 nm, which have a width of 16 nm, allowing the detection of subtle variations in the spectral response of vegetation in this red-edge region. Only 50 sites of interest around the world were chosen for the acquisition of VEN $\mu$ S satellite images, which present different vegetation and land uses. Itatinga station was selected as one of these acquisition sites. The images have a spatial resolution of 5.3 meters, a temporal resolution of 2 days, and a spectral resolution with 12 narrow bands, but we excluded band 1 from the analysis due to the high number of pixels without information (Table S1). We obtained the images from the Theia Land Data Centre (CNES). The images were already processed (geometric and radiometric corrections including atmospheric correction, cloud and cloud shadow mask) and ready to use. More information about the VEN $\mu$ S satellite can be found at [Theia \(CNES\) website](#).

In order to obtain a better characterization of the classes, we used two images, from 17/August/2019 and 06/March/2020, representing the main seasons of the year, winter (dry season, deciduous trees without leaves) and summer (rainy season) respectively (Figure S1). We extracted the values of each band of the multispectral images of the two seasons according to each class and compared the spectral response from different tree cover classes and different seasons (Figs. 5 and 6).

### 2.2.3. Model attributes

To generate the classification model, we used the reflectance values of each band of the satellite images as independent variables. In addition, we also generated new layers totaling 66 independent variables (Table 2). The methodology for each variable generated is described in the following sections.

Table 2. Number of variables used to generate the model.

Layer	Number of variables
Winter bands	11
Summer bands	11
Winter vegetation indices	6
Summer vegetation indices	6
Delta layers	6
Textural features	18
Winter alpha diversity	1
Summer alpha diversity	1
Winter PCA components	3
Summer PCA components	3

### 2.2.3.1. Vegetation indices and Delta layers

We calculated six vegetation indices using the reflectance values of the VEN $\mu$ S satellite bands (Table 3), using the R software (R Core Team, 2022). We preferentially selected indices that use bands located in the “red edge” region or associate high absorption bands (red spectral band) with high reflectance bands (infrared spectral band). These indices are related to the physical-chemical properties of the vegetation cover and can contribute to differentiate the tree cover classes in the classification model. These vegetation indices were generated for both seasons of the year and identified with the name of the index and the suffixes “\_winter” and “\_summer” (e.g. “NDVI\_winter”).

We calculated the Delta layers from the subtraction between the layers of the summer vegetation indices and the winter vegetation indices, using the “Raster Calculator” tool of the ArcGIS software (ArcGIS, 2021) and being identified with the name of the index and the suffix “\_delta” (e.g. “NDVI\_delta”). We generated these vegetation indices seasonal changes because they could differentiate tree cover classes in the classification model. Thus, classes that undergo changes in the dry season, such as leaf fall (e.g. semideciduous seasonal forest), have higher Delta values.

Table 3. Description of the vegetation indices used in the study, with their respective names, bands (labeled as  $\rho$  and the spectral band center), formulas used, and bibliographic references.

<b>Variable</b>	<b>Name</b>	<b>Bands</b>	<b>Formula</b>	<b>Reference</b>
CLre	<i>Red Edge Chlorophyll Index</i>	9, 11	$(\rho_{865} / \rho_{742}) - 1$	(Roberts et al., 2016)
EVI	<i>Enhanced Vegetation Index</i>	2, 6, 11	$2.5 * (\rho_{865} - \rho_{620}) / ((\rho_{865} + (6 * \rho_{620}) + (7.5 * \rho_{443})) + 1)$	(Roberts et al., 2016)
NDVI	<i>Normalized Difference Vegetation Index</i>	6, 11	$(\rho_{865} - \rho_{620}) / (\rho_{865} + \rho_{620})$	(Bar-Massada and Svir, 2020)
NDVIre	<i>Red Edge Normalized Difference Vegetation Index</i>	9, 10	$(\rho_{782} - \rho_{742}) / (\rho_{782} + \rho_{742})$	(Bar-Massada and Svir, 2020)
REIP	<i>Red Edge Inflection Point</i>	7, 8, 9, 10	$702 + (40 * (((\rho_{667} + \rho_{782}) / 2) - \rho_{702}) / (\rho_{742} - \rho_{702})))$	(Bar-Massada and Svir, 2020)
SR	<i>Simple Ratio</i>	6, 11	$\rho_{865} / \rho_{620}$	(Roberts et al., 2016)

### 2.2.3.2. Texture layers

We used the textural layers as independent variables for the model to indicate the spatial variation of the values of each vegetation index and delta layer. In the textural layers, we calculated the pixel values from the standard deviation of the pixels around them within a 9x9 pixel moving window, using the “Focal Statistics” tool of the ArcGIS software. We performed tests with models composed of different window sizes with three vegetation indices (“REIP\_winter”, “EVI\_winter” and “NDVIre\_winter”) to find out the lowest error rate, where the 9x9 window presented the best results (Figure S2). We generated these textural layers to characterize the canopy heterogeneity, to facilitate the differentiation between homogeneous plantations and heterogeneous forest formations. Their identifications were made with the name of the indices and the suffix “\_win\_tex” for winter (e.g. “NDVI\_win\_tex”) and “\_sum\_tex” for summer (e.g. “NDVI\_sum\_tex”), and “\_delta\_tex” for delta layers (e.g. “NDVI\_delta\_tex”).

### 2.2.3.3. Spectral diversity layers

We generated the spectral diversity layers in R software using the “biodivMapR” package (Féret and Boissieu, 2020). This package uses the spectral species concept (Féret and Asner, 2014) to generate alpha diversity maps and spectral composition maps, where a principal component analysis (PCA) is performed with the reflectance values of the bands, and clusters are created from their principal components and treated as species. Thus, a spectral species map is generated where each pixel belongs to a cluster/species. The alpha diversity map is a raster image where pixel values are calculated using the “Shannon” biodiversity index within a 9x9 pixel moving window. The spectral composition map is generated from an RGB composition where the bands come from the first three main components of the PCA. Moreover, for a better understanding of how the classes behave in relation to the PCA main components, we performed a second PCA with the three main components and plotted a biplot to visualize the classes distribution (Figure 4). More information about the “biodivMapR” package can be found at Féret et al. (2020). We extracted the values of each class from the alpha diversity maps and spectral composition maps and used them as attributes for the model. Such variables were identified with the prefix “alpha\_” (e.g. “alpha\_winter”) and “PCoA” (e.g. “PCoA.1\_winter”, “PCoA.2\_winter” and “PCoA.3\_winter”).

#### 2.2.4. Data analysis

For the classification, we used the supervised algorithm Random Forest (RF), through the “randomForest” package (Liaw and Wiener, 2002) in the R software. For the settings, all metaparameter were set to their default values. This classifier is one of the most used machine learning algorithms in remote sensing studies mostly because of its accurate classification with few metaparameters easy to tune, ability to handle high data dimensionality and multicollinearity of predictors, and its relative robustness against over-fitting (Belgiu and Drăguț, 2016; Gislason et al., 2006). The RF algorithm consists of a combination of many decision trees. Each decision tree is trained independently on a subset of the dataset and a subset of predictor variables. The classification results are determined by the majority of votes cast by all trees (Breiman, 2001; Mellor et al., 2010; Pal, 2005).

To calibrate the model and assess the variability in classification accuracy, we trained and tested the model 30 times (iteration) using the 66 variables, in a database with 7,000 observations (1,000 observations for each tree cover class randomly selected from the sampling polygons), randomly choosing 650 pixels for each tree cover class in each iteration. New training (70%) and test (30%) samples were used in each iteration, in which when a pixel from a given polygon was picked to the training set, no pixel from this polygon goes to the test set. In other words, no polygon was into the training and testing samples at the same iteration. At each repetition, we calculated and stored the “F1 score” values for each class, the “Mean Decrease Accuracy” (MDA) value for each variable, and the classification confusion matrix. After the 30 repetitions, we calculated the mean overall accuracy and the mean confusion matrix, and plotted the boxplots for the “F1 score” and MDA values.

The “F1 score” is the most used metric to assess a test’s accuracy. The MDA represents how much accuracy the model would lose if the variable were removed, that is, the higher its value, the greater the importance of the variable. The confusion matrix allows the analysis of the classification performance, showing the producer’s accuracy in percentage, in addition to specifying which classes were confused with each other.

To evaluate the effect of adding textural and spectral diversity metrics to the model’s accuracy we also generated other models in 3 different combinations of variables to evaluate how the addition of new metrics would increase the model’s accuracy (Table 5). All these models were generated with the same methodology of the full model, with 30 iterations and cross-validation. In the first case, we only used the summer bands and the vegetation indices. In the second, we added the summer textural features. In the third, we added the summer

spectral diversity components. Finally, we compared them with the full model, which includes all attributes.

### **2.2.5. Thematic map**

We generated a thematic map with all the tree cover classes as a product of the classification. For its elaboration, we trained a model with the 7,000 observations database. After training, this model was applied on all the pixels in the image to generate a pixel-scale classification map. Then, we performed four post-processing steps to eliminate spurious pixels, all in ArcGIS, using the “Raster Calculator”, “Majority Filter”, “Boundary Clean”, and “Nibble” tools. We filled the saturated pixels without information with the value of the majority of pixels around them, inside a 5x5 window, using the “Raster Calculator” tool. To eliminate isolated pixels and small groups of pixels, we used the “Majority Filter” tool considering a 3x3 window, where groups with less than 5 contiguous pixels were replaced by the value of most pixels around them. We used the “Boundary Clean” tool to smooth the boundaries between zones, prioritizing larger zones to expand over smaller zones. Finally, we used the “Nibble” tool to replace the values of groups that contained less than 350 contiguous pixels with the value of neighboring pixels, eliminating small groups of pixels. In this way, at the end of all the post-processing stages, we obtained a final smoothed thematic map with all the identified classes.

## **2.3. Results**

### **2.3.1. Tree cover classes characterization**

#### **2.3.1.1. Spectral diversity**

Alpha diversity and Spectral Composition maps created for both summer (Figure 2) and winter season (Figure S3) show which classes presented higher values of spectral diversity and the different compositions between classes. The classes “Old-growth semidecidual forest” and “Second-growth semidecidual forest” show the higher values of spectral diversity. In the winter, the “Eucalyptus monoculture” class presented higher values of diversity compared to summer, unlike the “Second-growth savanna woodland” class, which presented higher values in summer (Figure 3). The classes that presented the lowest spectral diversity values were “Bare soil” in winter and “Pine tree monoculture” in summer.

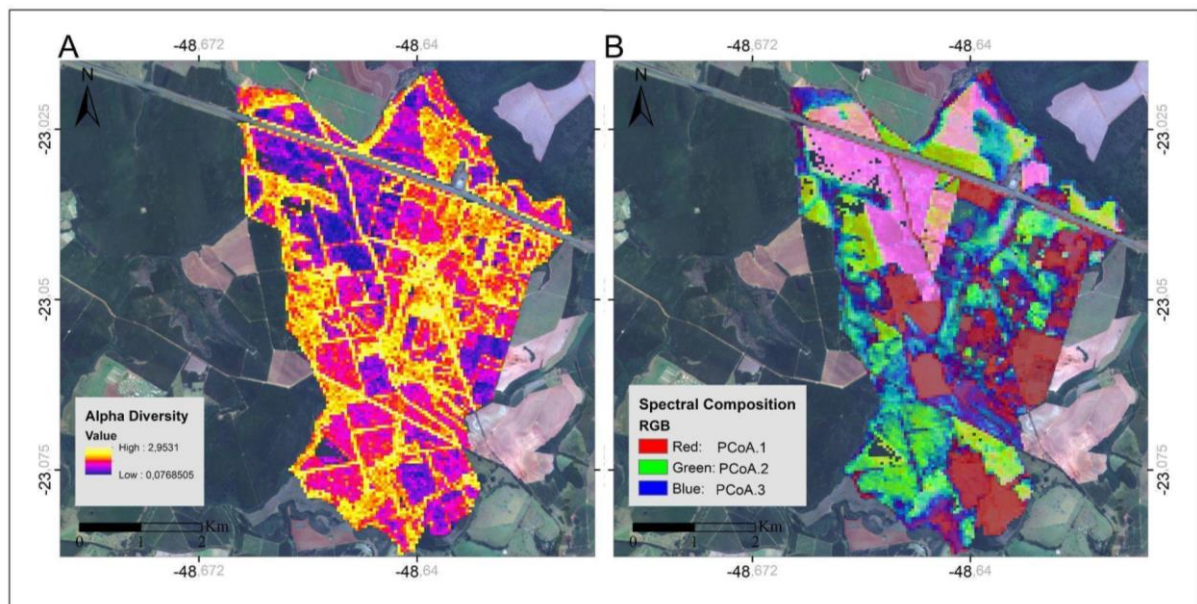


Figure 2. Summer alpha diversity map (A) and Spectral composition map (B) of the Itatinga station.

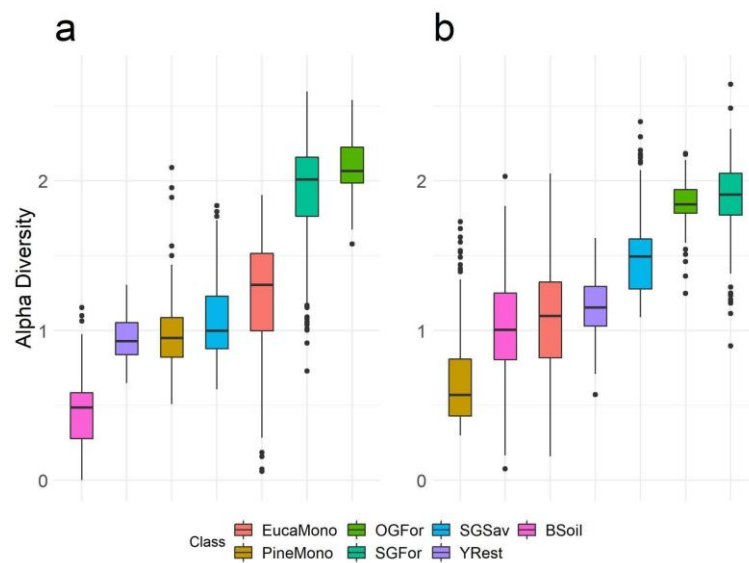


Figure 3. Alpha spectral diversity values of each tree cover class in the winter (a) and summer (b). Classes are: “Eucalyptus monoculture” (EucaMono), “Pine trees monoculture” (PineMono), “Old-growth semidecidual forest” (OGFor), “Second-growth semidecidual forest” (SGFor), “Second-growth savanna woodland” (SGSav), “Young restoration planting” (YRest) and “Bare soil” (BSoil).

The second PCA biplot graph shows the PCA main components composition used as variables to classify the tree cover classes, and allows to analyse which classes had similar composition in the summer and winter (Figure 4). In both seasons, the “Second-growth savanna woodland”, “Young restoration planting” and “Bare soil” classes showed a similar distribution and a low variance. The “Eucalyptus monoculture”, “Old-growth semidecidual forest” and “Second-growth semidecidual forest” classes showed a higher variance comparing



to the other classes. The “Old-growth semidecidual forest” and “Second-growth semidecidual forest” classes showed a similar distribution between each other. The “Pine trees monoculture” presented a different composition in between seasons.

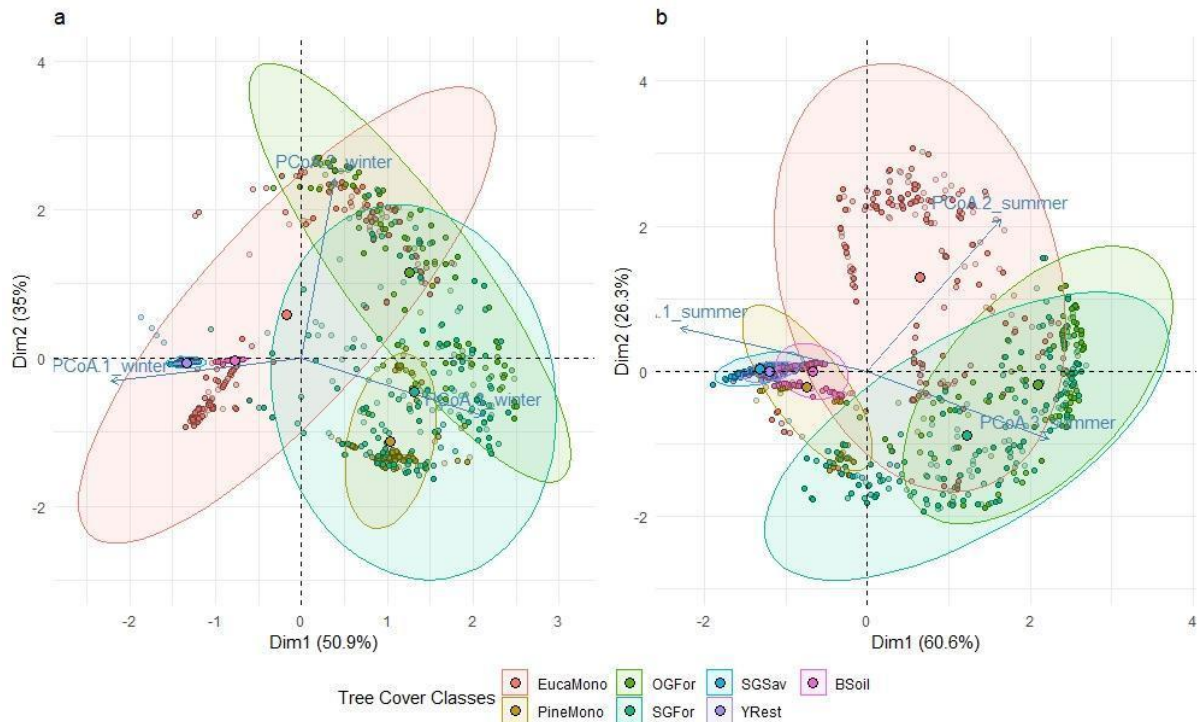


Figure 4. Biplot of the second PCA performed with the main components of the spectral composition map (Figure 2b), with the distribution of each tree cover class in the winter (a) and summer (b). Classes are: “Eucalyptus monoculture” (EucaMono), “Pine trees monoculture” (PineMono), “Old-growth semidecidual forest” (OGFor), “Second-growth semidecidual forest” (SGFor), “Second-growth savanna woodland” (SGSav), “Young restoration planting” (YRest) and “Bare soil” (BSoil).

### 2.3.1.2. Spectral behavior

The spectral curves make it possible to understand the spectral behavior of the different tree cover classes, by expressing the reflectance levels along the wavelengths, showing which classes have a similar behavior, which will have an influence in the classification (Figure 5). The “Second-growth savanna woodland” and “Young restoration planting” classes presented a similar behavior in all wavelengths and in both seasons. The “Eucalyptus monoculture”, “Pine tree monoculture”, “Old-growth semidecidual forest”, and “Second-growth semidecidual forest” classes showed similar behavior in the visible spectrum in both seasons, with low reflectance levels. However, these classes showed different behavior in the near infrared region (730 nm to 1000 nm). In general, all classes showed low variance in reflectance values in the visible region, except for the “Bare soil” class in summer. Regarding the infrared region, all classes showed a high variance in reflectance, where some

of the classes have overlapped. All vegetation classes showed a similar behavior in both seasons, with reflectance values slightly lower in the visible spectrum in summer. In the near-infrared region, the tree cover classes showed a higher reflectance in the summer than in winter, except the classes “Eucalyptus monoculture” and “Pine tree monoculture” that showed the same behavior in both seasons (Figure 5c). The “Old-growth semideciduous forest” and “Second-growth semideciduous forest” classes presented a very similar spectral behavior in the two seasons across the entire spectrum, as well as the “Second-growth savanna woodland” and “Young restoration planting” classes. In addition, the “Bare soil” class showed the greatest differentiation in the infrared region when comparing the two seasons.

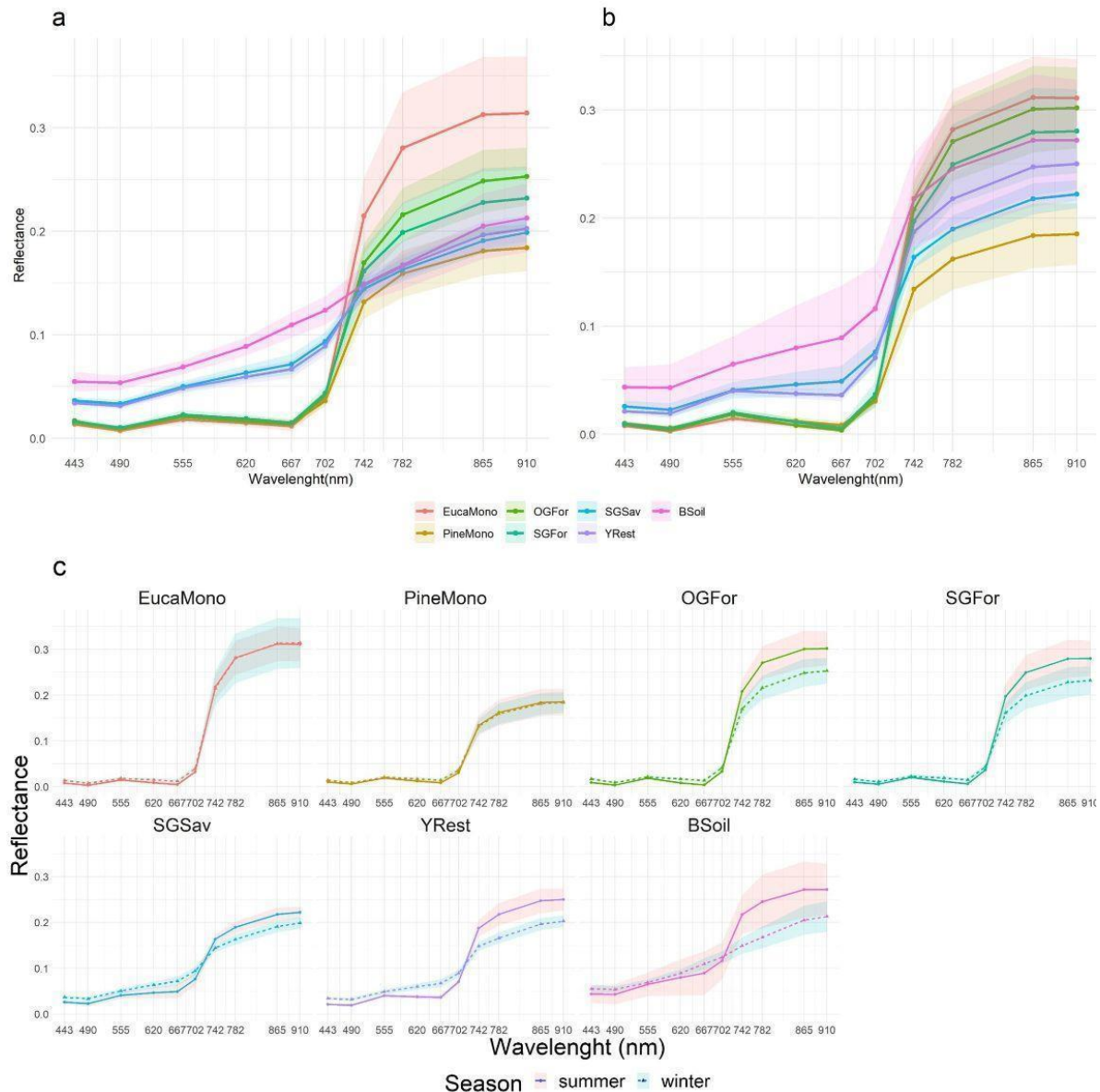


Figure 5. Average spectral curves and amplitude of variance of the different tree cover classes, from the multispectral images of the VEN $\mu$ S satellite in the winter (a) and summer (b). (c) Mean spectral curves during summer (continuous lines) and winter seasons (dotted lines) for each tree cover class. Classes are: “Eucalyptus monoculture” (EucaMono), “Pine trees monoculture” (PineMono), “Old-growth semidecidual forest” (OGFor), “Second-growth semidecidual forest” (SGFor), “Second-growth savanna woodland” (SGSav), “Young restoration planting” (YRest) and “Bare soil” (BSoil).

### 2.3.2. Tree cover classes classification

Considering the 30 iterations of the RF modeling, we reached a mean overall accuracy of 91.9% and average “F1 score” values above 0.8 for all tree cover classes (Figures 6 and 7). The confusion matrix shows which classes were more accurately classified, and which classes were confused. The “Second-growth semidecidual forest” class was the one with the lowest producer’s accuracy (74.4%), being confused with the “Pine tree monoculture” (0.4%), “Eucalyptus monoculture” (5.4%), and mainly “Old-growth semidecidual forest” (19.7%).

The “Old-growth semidecidual forest” class also showed lower producer’s accuracy (83.4%), being confused with the “Second-growth semidecidual forest” (16.6%). The “Second-growth savanna woodland” and “Young restoration planting” classes were confused with each other, even though they presented good producer’s accuracy values (95.2% and 96.4%). The “Bare soil” class was not confused with any class, presenting maximum producer’s accuracy (100%). The classes “Second-growth semidecidual forest” and “Old-growth semidecidual forest” were the most difficult to distinguish, with average “F1 score” values between 0.8 and 0.85 and the highest variance. The rest of the classes presented average values of “F1 score” above 0.95 and low variance (Figure 7).

	Target						
	EucaMono	PineMono	OGFor	SGFor	SGSav	YRest	BSoil
EucaMono	96.9%	1%	0%	5.4%	0%	0%	0%
PineMono	1.6%	99%	0%	0.4%	0%	0%	0%
OGFor	0%	0%	83.9%	19.7%	0%	0%	0%
SGFor	1.6%	0%	16.1%	74.4%	0%	0%	0%
SGSav	0%	0%	0%	0%	95.2%	1.5%	0%
YRest	0%	0%	0%	0%	4.8%	97.4%	0%
BSoil	0%	0%	0%	0%	0%	1%	100%

Figure 6. Normalized average confusion matrix indicating producer accuracy (i.e., the probability that a value in a given class was classified correctly), generated from the 30 iterations of the RF models. Classes are: “Eucalyptus monoculture” (EucaMono), “Pine trees monoculture” (PineMono), “Old-growth semidecidual forest” (OGFor), “Second-growth semidecidual forest” (SGFor), “Second-growth savanna woodland” (SGSav), “Young restoration planting” (YRest) and “Bare soil” (BSoil).

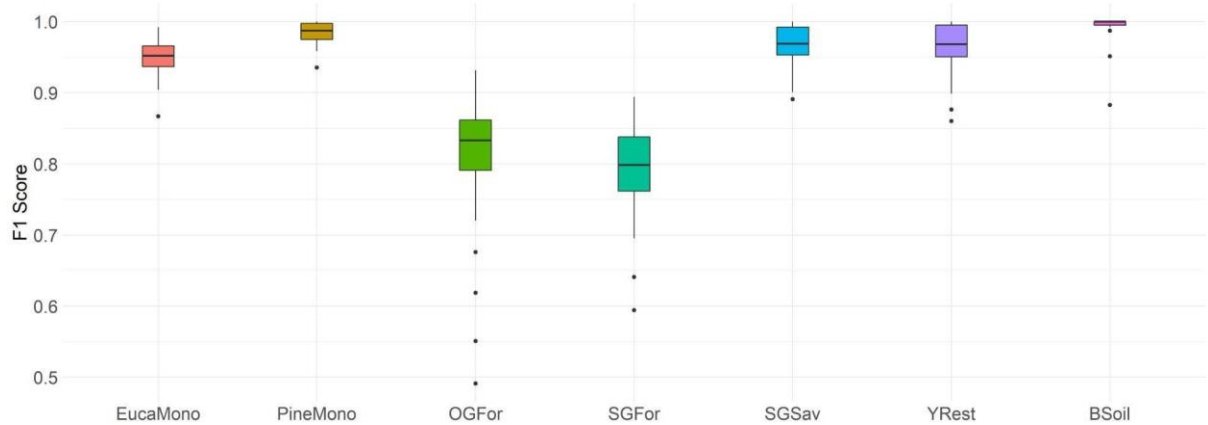


Figure 7. “F1 score” values of each tree cover class, calculated from the 30 RF models. Classes are: “Eucalyptus monoculture” (EucaMono), “Pine trees monoculture” (PineMono), “Old-growth semidecidual forest” (OGFor), “Second-growth semidecidual forest” (SGFor), “Second-growth savanna woodland” (SGSav), “Young restoration planting” (YRest) and “Bare soil” (BSoil).

After the 30 iterations of the RF model, we generated a ranking of the 66 variables used, based on their MDA values (Figure S4). The satellite bands that showed the greater MDA values were “B12\_summer”, “B9\_summer”, “B10\_summer”, “B11\_summer”, and “B12\_winter”, the rest of the bands showed lower values (Figure S4). Vegetation indices did not play a major role in the model, the most important being “EVI\_summer”, “NDVI\_summer”, “SR\_summer”, and “REIP\_winter”. The variables referring to the spectral diversity showed great MDA values. The textural variables of vegetation indexes and delta layers, in general, also expressed great MDA values. Among the most important variables are the textural metrics and spectral diversity variables (the top 10 variable’s importance are presented in Table 4).

Table 4. Presentation of the 10 most important variables for classification: average values of “Mean Decrease Accuracy” (yellow bars) and relative importance for each class (scaled green cells), calculated from the 30 iterations of the RF model. Classes are: “Eucalyptus monoculture” (EucaMono), “Pine trees monoculture” (PineMono), “Old-growth semidecidual forest” (OGFor), “Second-growth semidecidual forest” (SGFor), “Second-growth savanna woodland” (SGSav), “Young restoration planting” (YRest) and “Bare soil” (BSoil).

	Mean Decrease Accuracy	<i>EucaMono</i>	<i>PineMono</i>	<i>OGFor</i>	<i>SGFor</i>	<i>SGSav</i>	<i>YRest</i>	<i>BSoil</i>
1° <b>CLre_delta_tex</b>	45.7	0.38	0.25	1	0.55	0.95	0.99	0.26
2° <b>NDVI_sum_tex</b>	37	0.2	0.17	0.88	0.69	0.76	0.61	0.15
3° <b>alpha_summer</b>	31.8	0.47	0.45	0.42	0.69	0.72	0.66	0.21
4° <b>NDVlre_win_te</b>	31.2	0.36	0.33	0.97	0.29	0.19	0.16	0.17
5° <b>PCoA.1_summe</b>	30.9	0.31	0.41	0.58	0.48	0.65	0.46	0.24
6° <b>CLre_sum_tex</b>	29.5	0.56	0.32	0.82	0.49	0.41	0.32	0.19
7° <b>PCoA.2_winter</b>	26.7	0.48	0.3	0.78	0.77	0.42	0.54	0.51
8° <b>alpha_winter</b>	24.5	0.6	0.42	0.53	0.54	0.34	0.41	0.27
9° <b>NDVI_delta_tex</b>	23.4	0.13	0.24	0.31	0.35	0.58	0.54	0.2
10° <b>EVI_sum_tex</b>	23.2	0.51	0.59	0.51	0.73	0.31	0.25	0.14

After running the 3 other combinations of variables, we can notice that the addition of variables increases the model’s ability to distinguish the different tree cover classes (Table 5). When using only summer bands and vegetation indices, the overall accuracy of the model was 77%. Adding the summer textural features increased the accuracy by 8.5%, and adding the spectral diversity attributes increased an additional 2.1%. Finally, when comparing “Comb. 1” with the “Full Model”, there was an addition of 14.9% on the model’s overall accuracy.

Table 5. Description of the three combinations with different attributes configuration and their overall accuracy.

<b>Layer</b>	<b>Comb. 1</b>	<b>Comb. 2</b>	<b>Comb. 3</b>	<b>Full Model</b>
Winter bands (11)				X
Summer bands (11)	X	X	X	X
Winter vegetation indices (6)				X
Summer vegetation indices (6)	X	X	X	X
Delta layers (6)				X
Winter textural features (6)				X
Summer textural features (6)		X	X	X
Delta textural features (6)				X
Winter alpha diversity (1)				X
Summer alpha diversity (1)			X	X
Winter PCA components (3)				X
Summer PCA components (3)			X	X
<b><i>OVERALL ACCURACY</i></b>	<b><i>77%</i></b>	<b><i>85.5%</i></b>	<b><i>87.6%</i></b>	<b><i>91.9%</i></b>

### **2.3.2.1. Thematic map**

In the final classified thematic map, produced from the RF model, the smoothing steps helped to produce a map with less noise, eliminating most of the misclassified pixels and smoothing the divisions between zones (Figures 8). Thus, at the end of the study, we obtained a smoothed final thematic map, where we can observe the location of each vegetation class according to the chosen class.

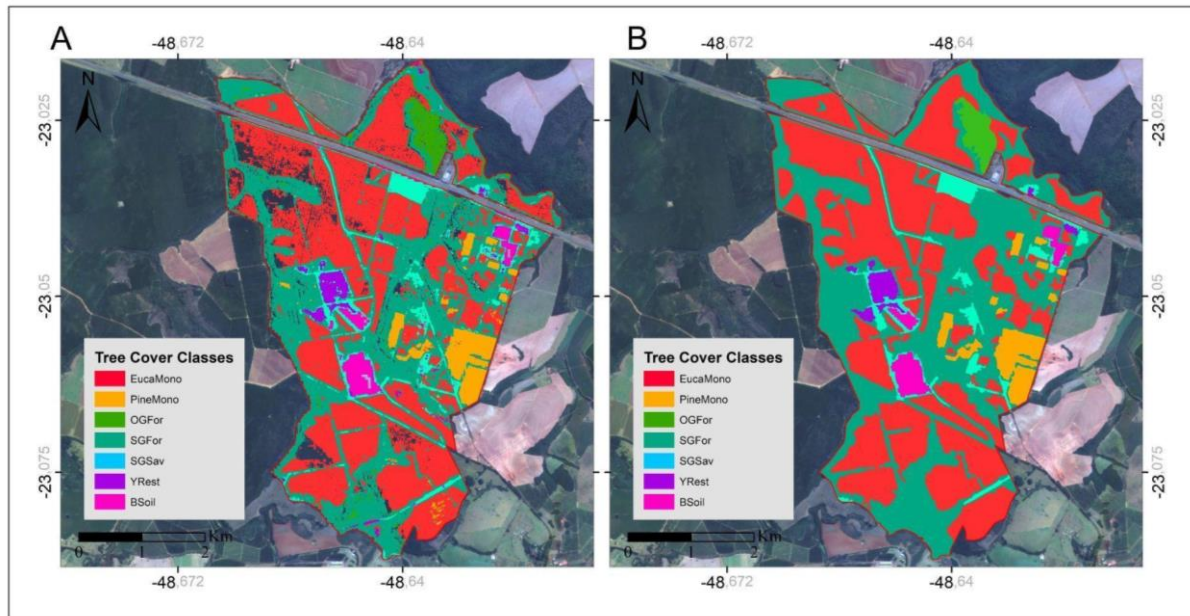


Figure 8. Thematic maps with classified tree cover classes, produced from the classification model, before (A) and after (B) the smoothing steps. Classes are: “Eucalyptus monoculture” (EucaMono), “Pine trees monoculture” (PineMono), “Old-growth semidecidual forest” (OGFor), “Second-growth semidecidual forest” (SGFor), “Second-growth savanna woodland” (SGSav), “Young restoration planting” (YRest) and “Bare soil” (BSoil).

## 2.4. Discussion

We aimed at evaluating the potential of high spatial and finer spectral resolution multispectral images from the VEN $\mu$ S satellite to perform supervised classification of contrasted tree cover classes, using the RF machine learning algorithm. To do so, tree cover class characterization was based on their spectral behavior and diversity, generating vegetation indices, delta layers, textural layers, and spectral diversity layers. We obtained high accuracy values (91.9%) and “F1 score” for all classes, which variables were most important for the accuracy of the classification, and finally a description of eventual confusion between tree cover classes.

The “Eucalyptus monoculture”, “Old-growth semidecidual forest”, “Second-growth semidecidual forest”, and “Pine tree monoculture” classes showed similar spectral behavior (i.e. high absorption), within the visible spectrum range and distinct behavior in the near-infrared region, but the high variance in this region made these classes overlap, preventing for using simple classification techniques only based on reflectance spectra. The similarity of the spectral response, mainly between the “Old-growth semidecidual forest” and “Second-growth semidecidual forest” classes, was probably due to their similar structure, with a closed canopy and high leaf density. Kalacska et. al. (2006) and Cao et. al. (2015) obtained similar results when carrying out studies in tropical dry forests at different stages of succession (initial,



intermediate, and late) using hyperspectral images, where both observed that forests in the intermediate and late stages of succession showed very similar spectral behavior in the visible and near-infrared region, but distinct in the short-wave infrared region, which is not contemplated in our study. The "Second-growth savanna woodland" and "Young restoration planting" classes also showed similar behavior, probably due to their low canopy height and low density of individuals, in addition to having a similar behavior to the "Bare soil" class in the near-infrared region, probably caused by their amount of exposed soil. As restoration plantings develop, we expect their spectral behavior will get similar to that of second-growth forests, as they have similar structure and species diversity (César et al., 2018).

When comparing the spectral behavior of the tree cover classes in the two seasons, the "Eucalyptus monoculture" and "Pine tree monoculture" classes did not significantly change, probably because of the date of the images were not at the minimum leaf area index caused, by the delay between the climate conditions and fisiologic response. On the other hand, the other classes showed higher reflectance values in the infrared region in summer than in winter, possibly caused by the greater amount of leaves (Weishampel et. al., 1996; Lee et. al., 2004). Regarding the spectral diversity profiles, the "Old-growth semidecidual forest" and "Second-growth semidecidual forest" classes presented the highest alpha diversity values and highest variance in the values of the principal components in the two seasons, which was expected because of their heterogeneous canopy and high species diversity. In the spectral composition maps (Figure 2B and S3B), we can observe that some Eucalyptus stands showed different compositions of principal components that might be caused by the different species, ages and managements, which explains the high variability in Figure 4. In addition, when observing the spectral diversity variables in the importance ranking (Table 4), the variables computed on the rainy season image (summer) showed more importance, probably due to the greater presence of leaves when compared to the dry season where some individuals shed their leaves.

The textural, delta, and spectral diversity layers were relevant in the classification with the highest MDA values. The high MDA values of the texture layers indicate the importance of analyzing the canopy heterogeneity to better characterize the tree cover classes (Table 4). Kim et. al. (2009) showed the importance of using textural metrics when classifying tree cover classes in the state of North Carolina (USA) using the combination of several textural metrics, obtaining an overall accuracy of 83%. In our study, we used only one type of textural metric (standard deviation), which highlights the possibility of improving the classification by adding other textural metrics (e.g. mean, homogeneity, correlation, contrast). The presence of

variables from the two seasons shows the importance of using images from different moments of the year for the accuracy of the model, as it allows for characterizing the canopy in terms of structural and phenological changes. Table 5 shows the importance of adding textural, seasonal and spectral diversity features in the classification analysis, in which the full model showed a 14.9% higher accuracy when compared to the model with only bands and vegetation indices.

Tottrup (2003), when classifying six tropical tree cover classes in the province of Nghe An (Vietnam), showed that the use of only two images at different times of the year allows for achieving an accuracy 10-20% greater than when using only one of them. Zhu and Liu (2014) also obtained greater accuracy when using five images (85.26%) instead of just one (63.13%) when classifying three tree cover classes in Ohio (USA). The MapBiomass initiative shows that it is possible to use multitemporal images of different moments, applying temporal filters to improve the classification of land use (Azevedo et al., 2019). At the same time, alpha diversity and spectral composition variables also presented high MDA values, showing their high capacity for characterizing tree cover classes. Gastauer et. al. (2022) also used the “biodivMapR” package to assess the environmental quality of mining areas undergoing restoration in the Amazon using vegetation attributes related to structure, diversity, and ecological processes, reaching an overall accuracy of 83% and demonstrated how the information concerning spectral diversity can be useful in vegetation studies. Ultimately, we highlighted the great importance of data manipulation methods to generate new variables to compose the model, where only the use of band reflectance would not be enough to characterize the tree cover classes and reach such a degree of accuracy.

In our study, the VEN $\mu$ S images performed well in the classification due to their characteristics of high spatial and spectral resolution compared to other common satellites (e.g. Landsat, Sentinel), but it has the disadvantage of having only a few acquisition sites. Multitemporal images have the advantage of large area coverage and high temporal resolution, in addition to allowing the measurement of the spectral response and, consequently, the spectral diversity of tree cover classes, which were very useful in this study. However, optical data do not provide information about the structure of the forest like data from active sensors that measure the structure of vegetation in a three-dimensional way, such as Lidar and Radar data (Almeida et al., 2019; Drezet and Quegan, 2007; Kimball et al., 2004; Lausch et al., 2017; Smith et al., 2009; Torre-Tojal et al., 2022). Our study was restricted to the use of variables from the multispectral images of the VEN $\mu$ S satellite, but it is important to emphasize the possibility of merging data from different sources to improve the

classification. Several authors highlight the potential of optical data fusion (RGB, multispectral and hyperspectral images), Radar, and/or Lidar for studies related to land use classification and monitoring of structural attributes of forests, seeking to achieve the best characterization of the vegetation (Almeida et al., 2021; Erdody and Moskal, 2010; García et al., 2018; Luo et al., 2017; Qi et al., 2019; Sankey et al., 2017). Jin and Mountrakis (2022) performed the land use classification by testing different combinations of data sources, in addition to performing a literature review with 75 studies of land use and occupation carried out between 2000 and 2021 that used the fusion of multi-source data and different machine learning algorithms, where the greatest discriminative power was found with the fusion of Landsat 5/TM, SAR (ALOS-1/PALSAR) and Lidar (LVIS) images.

Despite the good accuracy in distinguishing the classes, this study was restricted to the classification of generalist tree cover classes, without considering in-depth details regarding the composition, structure, age, position in the landscape and function of the forest fragments. Therefore, there is an opportunity to carry out future studies aimed at identifying tree cover classes using multispectral and multitemporal images, together with data from other sources, to achieve a greater degree of specificity, such as forests established from different restoration practices (e.g. natural regeneration, mixed restoration plantations, abandoned monocultures), different successional stages, and/or commercial plantations composed of different species and managements. Finally, our study showed that the combination of high spatial and finer spectral resolution multispectral images, different data manipulation techniques, and machine learning algorithms have great potential to assist the classification of tree cover classes across restored forest landscapes, which is expected to be the first step towards the assessment of biodiversity and ecosystem functions. Once the main tree cover classes of a FLR program are identified, further remote sensing approaches, like Lidar technology, and in-deep field assessments can be performed to advance evaluation of FLR benefits for nature and people. Ultimately, the fusion of all of these types of data, together with the use of innovative approaches to data processing, can result in novel ways to assess restoration performance and open new avenues to upscale monitoring, bridging the gap between FLR expectations and achieved goals.

## References

- Almeida, D.R.A., Almeyda Zambrano, A.M., Broadbent, E.N., Wendt, A.L., Foster, P., Wilkinson, B.E., Salk, C., Papa, D. de A., Stark, S.C., Valbuena, R., Gorgens, E.B., Silva, C.A., Brancalion, P.H.S., Fagan, M., Meli, P., Chazdon, R., 2020. Detecting successional changes in tropical forest structure using GatorEye drone-borne lidar. *Biotropica* 52, 1155–1167. doi:10.1111/btp.12814
- Almeida, D.R.A., Stark, S.C., Chazdon, R., Nelson, B.W., Cesar, R.G., Meli, P., Gorgens, E.B., Duarte, M.M., Valbuena, R., Moreno, V.S., Mendes, A.F., Amazonas, N., Gonçalves, N.B., Silva, C.A., Schietti, J., Brancalion, P.H.S., 2019. The effectiveness of lidar remote sensing for monitoring forest cover attributes and landscape restoration. *Forest Ecology and Management* 438, 34–43. doi:10.1016/j.foreco.2019.02.002
- Almeida, D.R.A. de, Broadbent, E.N., Ferreira, M.P., Meli, P., Zambrano, A.M.A., Gorgens, E.B., Resende, A.F., de Almeida, C.T., do Amaral, C.H., Corte, A.P.D., Silva, C.A., Romanelli, J.P., Prata, G.A., de Almeida Papa, D., Stark, S.C., Valbuena, R., Nelson, B.W., Guillemot, J., Féret, J.-B., Chazdon, R., Brancalion, P.H.S., 2021. Monitoring restored tropical forest diversity and structure through UAV-borne hyperspectral and lidar fusion. *Remote Sensing of Environment* 264, 112582. doi:10.1016/j.rse.2021.112582
- ArcGIS [GIS software]. Version 10.3. Redlands, CA: Environmental Systems Research Institute, Inc., 2022
- Azevedo, T. D., Rosa, M. R., Shimbo, J. Z., Martins, E. V., Oliveira, M. D., 2019. Annual Deforestation Report of Brazil 2019, MapBiomass.
- Bar-Massada, A., Sviri, A., 2020. Utilizing vegetation and environmental new micro spacecraft (venµs) data to estimate live fuel moisture content in israel's mediterranean ecosystems. *IEEE J. Sel. Top. Appl. Earth Observations Remote Sensing* 13, 3204–3212. doi:10.1109/JSTARS.2020.3001677
- Battie-Laclau, P., Laclau, J.-P., Domec, J.-C., Christina, M., Bouillet, J.-P., de Cassia Piccolo, M., de Moraes Gonçalves, J.L., Moreira, R.M.E., Krusche, A.V., Bouvet, J.-M., Nouvellon, Y., 2014. Effects of potassium and sodium supply on drought-adaptive mechanisms in *Eucalyptus grandis* plantations. *New Phytol.* 203, 401–413. doi:10.1111/nph.12810
- Belgiu, M., Drăguț, L., 2016. Random forest in remote sensing: A review of applications and future directions. *ISPRS Journal of Photogrammetry and Remote Sensing* 114, 24–31. doi:10.1016/j.isprsjprs.2016.01.011
- Breiman, L., 2001. *Random Forests*. Springer Science and Business Media LLC. doi:10.1023/a:1010933404324
- Cao, S., Yu, Q., Sanchez-Azofeifa, A., Feng, J., Rivard, B., Gu, Z., 2015. Mapping tropical dry forest succession using multiple criteria spectral mixture analysis. *ISPRS Journal of Photogrammetry and Remote Sensing* 109, 17–29. doi:10.1016/j.isprsjprs.2015.08.009

César, R.G., Moreno, V.S., Coletta, G.D., Chazdon, R.L., Ferraz, S.F.B., de Almeida, D.R.A., Brancalion, P.H.S., 2018. Early ecological outcomes of natural regeneration and tree plantations for restoring agricultural landscapes. *Ecol. Appl.* 28, 373–384. doi:10.1002/eap.1653

Chaves, R.B., Durigan, G., Brancalion, P.H.S., Aronson, J., 2015. On the need of legal frameworks for assessing restoration projects success: new perspectives from São Paulo state (Brazil). *Restor. Ecol.* 23, 754–759. doi:10.1111/rec.12267

Dedieu, G., Karnieli, A., Hagolle, O., Jeanjean, H., Cabot, F., Ferrier, P., Yaniv, Y., 2006. VENUS: A joint Israel–French earth observation, scientific mission with high spatial and temporal resolution capabilities. In *Second Recent Advances in Quantitative Remote Sensing Symposium*.

de Oliveira Santos, C.L.M., Lamparelli, R.A.C., Dantas Araújo Figueiredo, G.K., Dupuy, S., Boury, J., Luciano, A.C. dos S., Torres, R. da S., le Maire, G., 2019. Classification of Crops, Pastures, and Tree Plantations along the Season with Multi-Sensor Image Time Series in a Subtropical Agricultural Region. *Remote Sens (Basel)* 11, 334. doi:10.3390/rs11030334

Drezet, P.M.L., Quegan, S., 2007. Satellite-based radar mapping of British forest age and Net Ecosystem Exchange using ERS tandem coherence. *Forest Ecology and Management* 238, 65–80. doi:10.1016/j.foreco.2006.09.088

Erdody, T.L., Moskal, L.M., 2010. Fusion of LiDAR and imagery for estimating forest canopy fuels. *Remote Sensing of Environment* 114, 725–737. doi:10.1016/j.rse.2009.11.002

Féret, J.-B., Asner, G.P., 2014. Mapping tropical forest canopy diversity using high-fidelity imaging spectroscopy. *Ecol. Appl.* 24, 1289–1296. doi:10.1890/13-1824.1

Féret, J., Boissieu, F., 2020. biodivMapR: An R package for  $\alpha$ - and  $\beta$ -diversity mapping using remotely sensed images. *Methods Ecol. Evol.* 11, 64–70. doi:10.1111/2041-210X.13310

García, M., Saatchi, S., Ustin, S., Balzter, H., 2018. Modelling forest canopy height by integrating airborne LiDAR samples with satellite Radar and multispectral imagery. *International Journal of Applied Earth Observation and Geoinformation* 66, 159–173. doi:10.1016/j.jag.2017.11.017

Gastauer, M., Nascimento, W.R., Caldeira, C.F., Ramos, S.J., Souza-Filho, P.W.M., Féret, J.-B., 2022. Spectral diversity allows remote detection of the rehabilitation status in an Amazonian iron mining complex. *International Journal of Applied Earth Observation and Geoinformation* 106, 102653. doi:10.1016/j.jag.2021.102653

Gislason, P.O., Benediktsson, J.A., Sveinsson, J.R., 2006. Random Forests for land cover classification. *Pattern Recognit. Lett.* 27, 294–300. doi:10.1016/j.patrec.2005.08.011

Herscovitz, J., Barnett, D.L., 2007. 2.4.1 Decision Analysis for Design Trades for A Combined Scientific-Technological Mission Orbit on Venus Micro Satellite. *INCOSE International Symposium* 17, 367–382. doi:10.1002/j.2334-5837.2007.tb02881.x

Herscovitz, J., Karnieli, A., 2008. VEN $\mu$ S Program: Broad and New Horizons for Super-Spectral Imaging and Electric Propulsion Missions for a Small Satellite.

Houet, T., Verburg, P.H., Loveland, T.R., 2010. Monitoring and modelling landscape dynamics. *Landscape Ecol.* 25, 163–167. doi:10.1007/s10980-009-9417-x

Hua, F., Bruijnzeel, L.A., Meli, P., Martin, P.A., Zhang, J., Nakagawa, S., Miao, X., Wang, W., McEvoy, C., Peña-Arancibia, J.L., Brancalion, P.H.S., Smith, P., Edwards, D.P., Balmford, A., 2022. The biodiversity and ecosystem service contributions and trade-offs of forest restoration approaches. *Science* 376, 839–844. doi:10.1126/science.abl4649

Jin, H., Mountrakis, G., 2022. Fusion of optical, radar and waveform LiDAR observations for land cover classification. *ISPRS Journal of Photogrammetry and Remote Sensing* 187, 171–190. doi:10.1016/j.isprsjprs.2022.03.010

Kalacska, M., Sanchez-Azofeifa, G.A., Rivard, B., Caelli, T., White, H.P., Calvo-Alvarado, J.C., 2007. Ecological fingerprinting of ecosystem succession: Estimating secondary tropical dry forest structure and diversity using imaging spectroscopy. *Remote Sensing of Environment* 108, 82–96. doi:10.1016/j.rse.2006.11.007

Kimball, J.S., McDonald, K.C., Running, S.W., Frolking, S.E., 2004. Satellite radar remote sensing of seasonal growing seasons for boreal and subalpine evergreen forests. *Remote Sensing of Environment* 90, 243–258. doi:10.1016/j.rse.2004.01.002

Kim, M., Madden, M., Warner, T.A., 2009. Forest Type Mapping using Object-specific Texture Measures from Multispectral Ikonos Imagery: Segmentation Quality and Image Classification Issues. *Photogrammetric Engineering and Remote Sensing* Vol. 75, 819–829.

Lamb, D., 2018. Undertaking large-scale forest restoration to generate ecosystem services. *Restor. Ecol.* 26, 657–666. doi:10.1111/rec.12706

Lausch, A., Erasmi, S., King, D., Magdon, P., Heurich, M., 2017. Understanding Forest Health with Remote Sensing-Part II—A Review of Approaches and Data Models. *Remote Sens (Basel)* 9, 129. doi:10.3390/rs9020129

Lee, K. S., Park, Y. I., Kim, S. H., Park, J. H., Woo, C. S., Jang, K. C., 2004. Remote sensing estimation of forest LAI in close canopy situation. In *Geo-Imagery Bridging Continents XXth ISPRS Congress*, pp. 12-23.

Lewis, S.L., Wheeler, C.E., Mitchard, E.T.A., Koch, A., 2019. Restoring natural forests is the best way to remove atmospheric carbon. *Nature* 568, 25–28. doi:10.1038/d41586-019-01026-8

Liaw, A., Wiener, M., 2002. Classification and Regression by randomForest. *R News* 2(3), 18–22.

Luo, S., Wang, C., Xi, X., Pan, F., Peng, D., Zou, J., Nie, S., Qin, H., 2017. Fusion of airborne LiDAR data and hyperspectral imagery for aboveground and belowground forest biomass estimation. *Ecological Indicators* 73, 378–387. doi:10.1016/j.ecolind.2016.10.001

- Mellor, A., Haywood, A., Jones, S., Wilkes, P., 2012. Forest classification using random forests with multisource remote sensing and ancillary GIS data. In Proceedings of 16th Australian Remote Sensing and Photogrammetry Conference, Vol. 2728.
- Pal, M., 2005. Random forest classifier for remote sensing classification. *Int. J. Remote Sens.* 26, 217–222. doi:10.1080/01431160412331269698
- Qi, W., Lee, S.-K., Hancock, S., Luthcke, S., Tang, H., Armston, J., Dubayah, R., 2019. Improved forest height estimation by fusion of simulated GEDI Lidar data and TanDEM-X InSAR data. *Remote Sensing of Environment* 221, 621–634. doi:10.1016/j.rse.2018.11.035
- R Core Team, 2022. R: A language and environment for statistical computing. R Foundation for Statistical Computing. URL <https://www.R-project.org/>.
- Roberts, D. A., Roth, K. L., Perroy, R. L., 2016. 14 hyperspectral vegetation indices. *Hyperspectral remote sensing of vegetation*, 309.
- Sankey, T., Donager, J., McVay, J., Sankey, J.B., 2017. UAV lidar and hyperspectral fusion for forest monitoring in the southwestern USA. *Remote Sensing of Environment* 195, 30–43. doi:10.1016/j.rse.2017.04.007
- Smith, A.M.S., Falkowski, M.J., Hudak, A.T., Evans, J.S., Robinson, A.P., Steele, C.M., 2009. A cross-comparison of field, spectral, and lidar estimates of forest canopy cover. *Canadian Journal of Remote Sensing* 35, 447–459. doi:10.5589/m09-038
- Stanturf, J.A., Kleine, M., Mansourian, S., Parrotta, J., Madsen, P., Kant, P., Burns, J., Bolte, A., 2019. Implementing forest landscape restoration under the Bonn Challenge: a systematic approach. *Ann. For. Sci.* 76, 50. doi:10.1007/s13595-019-0833-z
- Temperton, V.M., Buchmann, N., Buisson, E., Durigan, G., Kazmierczak, L., Perring, M.P., Sá Dechoum, M., Veldman, J.W., Overbeck, G.E., 2019. Step back from the forest and step up to the Bonn Challenge: How a broad ecological perspective can promote successful landscape restoration. *Restor. Ecol.* 27, 705–719. doi:10.1111/rec.12989
- Torre-Tojal, L., Bastarrika, A., Boyano, A., Lopez-Guede, J.M., Graña, M., 2022. Above-ground biomass estimation from LiDAR data using random forest algorithms. *J. Comput. Sci.* 58, 101517. doi:10.1016/j.jocs.2021.101517
- Tottrup, C., 2004. Improving tropical forest mapping using multi-date Landsat TM data and pre-classification image smoothing. *Int. J. Remote Sens.* 25, 717–730. doi:10.1080/01431160310001598926
- Weishampel, J. F., Ranson, K. J., Harding, D. J., 1996. REMOTE SENSING OF FOREST CANOPIES, 17(1), 6–14. <http://www.jstor.org/stable/41759918>
- Wortley, L., Hero, J.-M., Howes, M., 2013. Evaluating Ecological Restoration Success: A Review of the Literature. *Restor. Ecol.* 21, 537–543. doi:10.1111/rec.12028

Zhu, X., Liu, D., 2014. Accurate mapping of forest types using dense seasonal Landsat time-series. *ISPRS Journal of Photogrammetry and Remote Sensing* 96, 1–11.  
doi:10.1016/j.isprsjprs.2014.06.012

## Supplementary Material

Bands	Center Wavelength (nm)	Bandwidth (nm)
B1	420	40
B2	443	40
B3	490	40
B4	555	40
B5	620	40
B6	620	40
B7	667	30
B8	702	24
B9	742	16
B10	782	16
B11	865	40
B12	910	20

Table S1. Bands of the multispectral images of the VEN $\mu$ S satellite, with their central wavelengths and width.

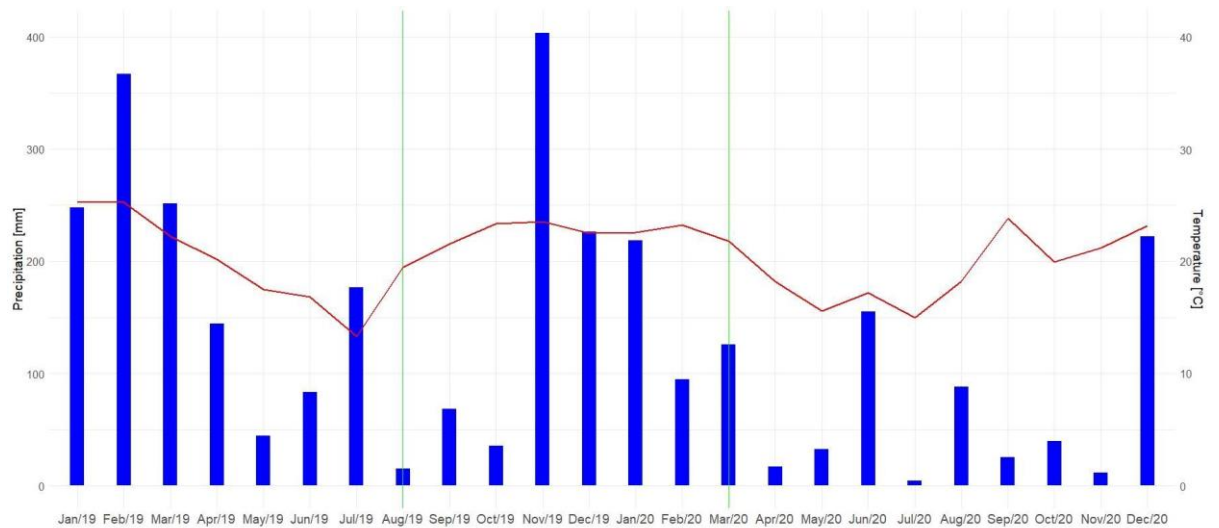


Figure S1. The monthly climatological graph in the years 2019 and 2020, with data from the Itatinga's Experimental Stations of Forest Sciences' meteorological station, with mean temperature (red line), accumulated monthly precipitation (blue bars), and date of the image used in this study (vertical green lines).



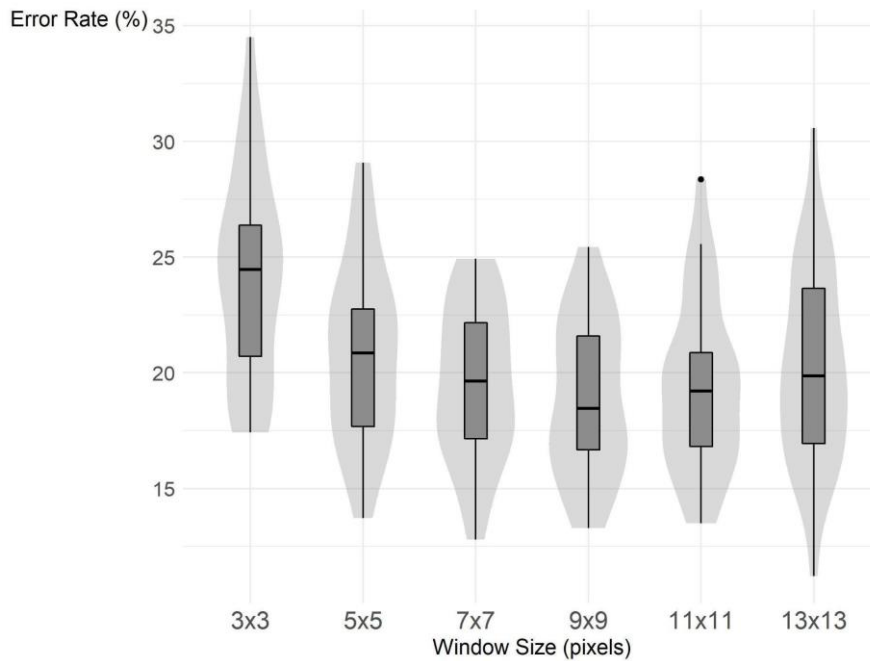


Figure S2. Boxplot of the error rate values in 30 iterations, testing the influence of the textural layers' moving window size on the model accuracy with three vegetation indexes (“REIP\_winter”, “EVI\_winter” and “NDVIre\_winter”).

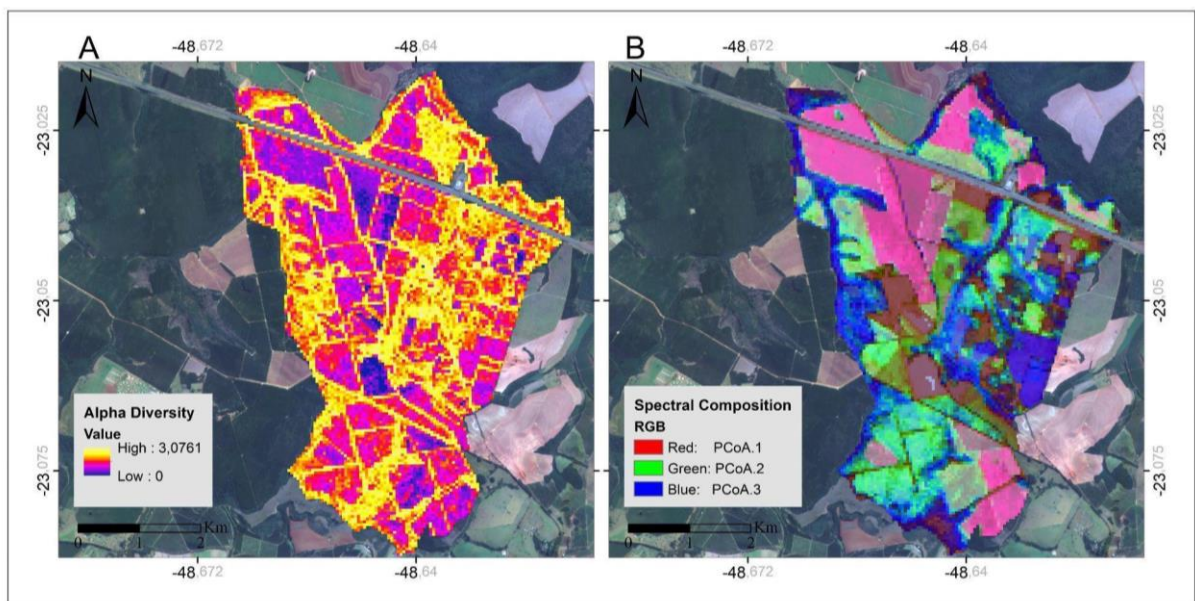


Figura S3. Winter alpha diversity map (A) and Spectral composition map (B) produced using the “biodivMapR” package.

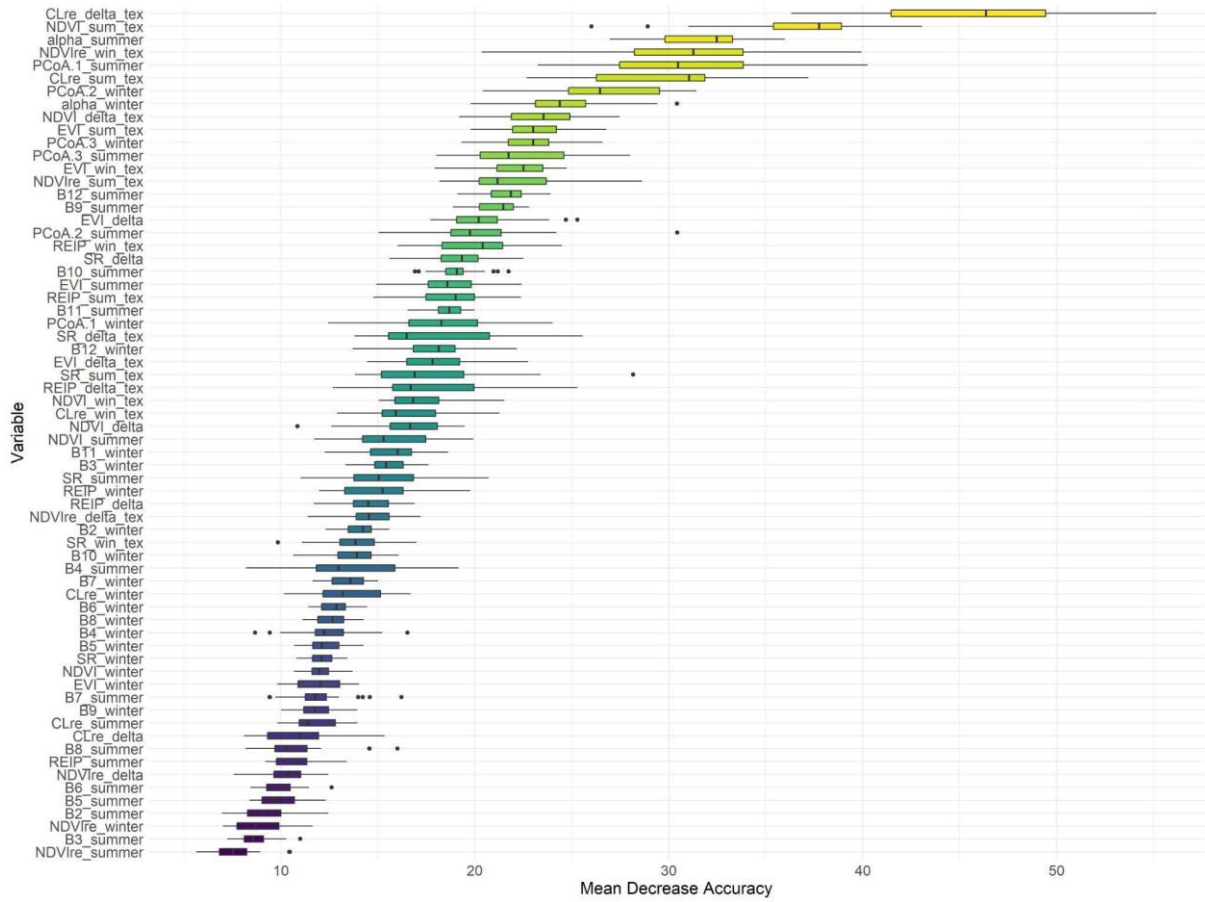


Figure S4. Boxplot of the “Mean Decrease Accuracy” values of all variables used in the study from the 30 RF models.



### **3. SECOND `D` OF REDD+ PROJECTS: APPLICATIONS OF UAV-LIDAR ON LOCAL DEGRADATION MONITORING**

#### **Abstract**

Forest monitoring is an essential stage in the management and maintenance of carbon projects targeting the Reduction of Emissions from Deforestation and Forest Degradation (REDD+) and climate change mitigation. Detecting forest degradation proves challenging due to its subtle and gradual nature, requiring detailed and periodic local monitoring efforts. Innovative remote sensing technologies, such as Light Detection and Ranging (LiDAR), have shown great potential in addressing these deficiencies. Quantifying emissions from degradation is a crucial aspect of REDD+ projects on the carbon market, as it allows for the accurate estimation of carbon stock in the project area. Additionally, it promotes credibility, transparency, and accountability, ensuring that projects embrace rigorous standards and guidelines. Therefore, the objective of this study was to assess the potential of LiDAR remote sensing technology to identify and monitor different sources of degradation in REDD+ projects and understand their effect on forest structure and carbon storage potential. For this purpose, we employed a statistical modeling of forest structural characteristics in relation to the distance from potential degradation sources (anthropized areas). This study was conducted on three rural properties that are part of an ongoing REDD+ project, located in the state of Acre/BR, southwestern region of the Brazilian Legal Amazon. Our findings have demonstrated that the impact of open areas on forest structure extends up to 50 meters, showcasing the remarkable resilience of the forests examined in this study. These results underscore the importance of further research to fully unlock the potential and promote the widespread adoption of UAV-LiDAR systems in the monitoring of REDD+ projects. This study has revealed the significant potential of LiDAR remote sensing technology for monitoring local degradation in REDD+ projects. The methodology utilized allowed for a comprehensive and detailed assessment of forest structure, offering replicable and periodic monitoring capabilities that enhance its effectiveness.

#### **Keywords:**

Amazon forest, Edge effect, Forest canopy structure, Carbon stock, Leaf area index

#### **3.1. Introduction**

Forest monitoring is an essential stage in the management and maintenance of carbon projects targeting the Reduction of Emissions from Deforestation and Forest Degradation (REDD+) and climate change mitigation. These activity is typically conducted during the initial stages of project development to stablish a baseline assessment of the forest's condition and identify potential threats, and is subsequently carried out periodically as part of the Measurement, Reporting, and Verification (MRV) process, where it enables the assessment of whether the project effectively prevents deforestation and forest degradation (De Sy et al., 2012; Goetz et al., 2015). (De Sy et al., 2012; Goetz et al., 2015). Presently, deforestation indicators can be derived from satellite imagery, allowing for the identification of abrupt land use changes and facilitating frequent monitoring across various spatial scales (McCracken et

al., 1999; de Espindola et al., 2012; Diniz et al., 2015; Silva et al., 2022; Ferrari et al., 2023). Conversely, detecting forest degradation proves challenging due to its subtle and gradual nature, requiring detailed and periodic local monitoring efforts (Goetz et al., 2015; Gao et al., 2020). Moreover, emissions from degraded forests can be substantial, equivalent to or even surpassing those resulting from deforestation, making their quantification indispensable (Aragão et al., 2014; Longo et al., 2016; Assis et al., 2020; Lapola et al., 2023). However, many REDD+ projects fail to include degradation as an emission source, resulting in its neglect and potentially underestimating overall emissions (Mertz et al., 2012; Silva Junior et al., 2021). The report issued by the United Nations Framework Convention on Climate Change (UNFCCC, 2014) in response to the Brazilian Forest Reference Emission Level (FREL) (MMA, 2014) also highlights the need for monitoring degradation to better understand its relationship with deforestation and its contribution to greenhouse gas emissions in the Amazon biome. Thus, heightened attention to forest degradation within REDD+ projects is warranted, accompanied by the development of comprehensive studies elucidating its impacts on forested areas, while encouraging the adoption of novel technologies and methodologies to enhance the efficiency and scalability of monitoring efforts.

Forests are considered degraded when they exhibit anthropogenic alterations in their structure, dynamics, biodiversity, and/or ecosystem services that are expected from them (Thompson et al., 2013). Forest degradation can occur in various forms, with selective logging, anthropogenic fires, grazing within the forests, and fuelwood/charcoal collection being its main direct sources (Hosonuma et al., 2012). Indirect disturbances also exist, such as edge effects resulting from land use change and forest fragmentation, as well as droughts and fires induced by climate change (Lapola et al., 2023). Some of these factors are more amenable to periodic monitoring using satellite imagery, while others may be more challenging to detect, such as selective logging and edge effects, as they cause changes in forest structure that are difficult to capture with passive sensors. The different sources and intensities of disturbances affect forest structure in distinct ways. Understanding how different degradation sources impact the forest and its ecosystem services is crucial for monitoring REDD+ projects (Cochrane and Schulze, 1999; Gerwing, 2002; Haugaasen et al., 2003; Broadbent et al., 2008; Rappaport et al., 2018; Yang et al., 2018). In this study, as no other sources of degradation were identified in the project areas, our focus was on detecting the presence of selective logging and assessing degradation caused by edge effects.

Unlike deforestation, which involves the clear-cutting of forests, selective logging refers to the extraction of specific commercial tree species. This practice causes damage to the

forest structure, altering its composition, biomass, and ecosystem services, while also increasing its vulnerability to droughts and fires (Asner et al., 2005; Asner et al., 2006; Broadbent et al., 2008). Therefore, the identification of this activity is crucial for REDD+ projects, as it has a direct impact on forest conservation and carbon stocks. Depending on the intensity of selective logging, its detection through satellite imagery becomes challenging, requiring the use of other sensors that allow for a more detailed observation of the changes in the forest structure (Rangel Pinagé et al., 2019). The document "VMD0015 - Methods for monitoring of GHG emissions and removals in REDD and CIW projects" (VCS, 2020), published by the leading certification body VERRA, presents a methodology for quantifying emissions resulting from degradation caused by selective logging through transect walks, searching for evidence of removed tree trunks. However, this field survey methodology is labor-intensive and low-yielding, being inefficient as it covers only a small portion of the project area and hampers periodic monitoring. Additionally, the lack of a comprehensive methodology that includes other sources of degradation, such as edge effects, may result in a potential underestimation of degradation emissions in REDD+ projects.

Degradation caused by edge effects follows the process of land use and land cover change in the Amazon biome, where agricultural and pasture areas replace forested areas (Broadbent et al., 2008; Silva Junior et al., 2021). Once opened, these areas gradually modify the microclimate at the forest edge, with increased temperature, decreased air and soil humidity, and intensified winds, causing changes in forest structure and its carbon stocks (Camargo and Kapos, 1995; Mesquita et al., 1999). Furthermore, the extent of edge infiltration is directly related to the type of land use, forest characteristics, matrix habitat, regional climate, and fragmentation intensity (Wuyts et al., 2008; Aragão et al., 2014; Goetz et al., 2015). Moreover, as edge effects impact the forest structure, they also affect canopy gap dynamics through tree mortality, branch breakage, and growth of secondary individuals. This simultaneous process of gap creation followed by plant regeneration is referred to as gap dynamics. Understanding this dynamics is crucial for assessing the integrity and level of forest degradation in REDD+ projects (Asner et al., 2013; Silva et al., 2019). Therefore, the high variability of edge effects underscores the need for their local-level monitoring, assessing their consequences on forests and carbon stocks for each individual REDD+ project (Broadbent et al., 2008).

Innovative remote sensing technologies, such as Light Detection and Ranging (LiDAR), have shown great potential in addressing these deficiencies. These technologies have modernized our way of observing forests, enabling the acquisition of previously

inaccessible information about forest structure and dynamics, as well as expanding our capacity to monitor them in various ways (Asner et al., 2013; Almeida et al., 2020). LiDAR is an active sensor that performs a laser scan of the forest, allowing for detailed characterization of its 3D structure, which is one of the main limitations of passive imaging sensors. This particularity of LiDAR enables the detection of changes in the vertical structure of the forest, enhancing forest monitoring and enabling more effective and detailed periodic monitoring. However, the document VMD0015 (VCS, 2020) does not present a specific methodology for the use of LiDAR data in degradation monitoring. Therefore, the objective of this study was to assess the potential of LiDAR remote sensing technology to identify and monitor different sources of degradation in REDD+ projects and understand their effect on forest structure and carbon storage potential. For this purpose, we employed two approaches: statistical modeling of forest structural characteristics in relation to the distance from potential degradation sources (anthropized areas) and gap analysis comparing the gap dynamics between forests near and far from anthropized areas. This study has practical implications related to the management of REDD+ projects, the ecology of land use change, and the use of innovative technologies for local degradation monitoring. Thus, we raised the following questions:

***(i) How to identify sources of degradation and quantify their emissions in REDD+ projects?***

We expect that the ability of LiDAR sensors to provide detailed characterization of the 3D forest structure will facilitate the identification of degradation sources that are challenging to monitor with optical sensors, such as selective logging and edge effects, and assist in measuring its modifications and in quantifying the emissions caused by these sources (Rangel Pinagé et al., 2019; Almeida et al., 2019). These measurements can be used to identify areas affected by selective logging and edge effects, and quantify the extent and severity of such degradation, by examining the transition zones between intact forests and adjacent land use types, providing insights into the extent and impact on forest ecosystems.

***(ii) How do anthropogenic areas alter canopy structure and carbon stocks in adjacent forests?***

We expect that the LiDAR sensor will allow us to identify the changes caused by the edge effect. Our hypothesis is that anthropogenic areas cause some level of disturbance in adjacent forests, resulting in alterations in their structure and carbon storage potential, but that these changes are quickly mitigated in preserved forests (Blanchard et al., 2023).

*(iii) What is the level of infiltration of degradation caused by anthropized areas?*

The infiltration of the edge effect in transition zones between anthropized and forested areas varies greatly depending on the intensity and duration of human activities, the proximity of the degraded areas to intact forests, the resilience of the ecosystem, and the attributes being assessed (Broadbent et al., 2008). We expect that in preserved forests, degradation will not infiltrate as intensely into the interior of the forest, altering the structure and carbon stocks of the forest only in the areas closest to the edge (Wuyts et al., 2008; Aragón et al., 2014; Almeida et al., 2019).

### **3.2. Material and Methods**

#### **3.2.1. Study Area**

This study was conducted on three rural properties that are part of an ongoing REDD+ project (accessed at <https://registry.verra.org/app/projectDetail/VCS/2551>), located in the state of Acre/BR, southwestern region of the Brazilian Legal Amazon (Figure 1). The occupation and opening of areas within these properties date back to the year 2008. The main vegetation type found is Open Ombrophilous Forest, which is considered a transitional vegetation with a relatively low and open canopy, presence of palm trees and bamboos, and occasional strong winds that can cause tree fall within the forest. Field walks were carried out, following the guidelines suggested in document MD0015 (VCS, 2020), along with aerial surveys using UAV-LiDAR in the zones adjacent to the open areas.



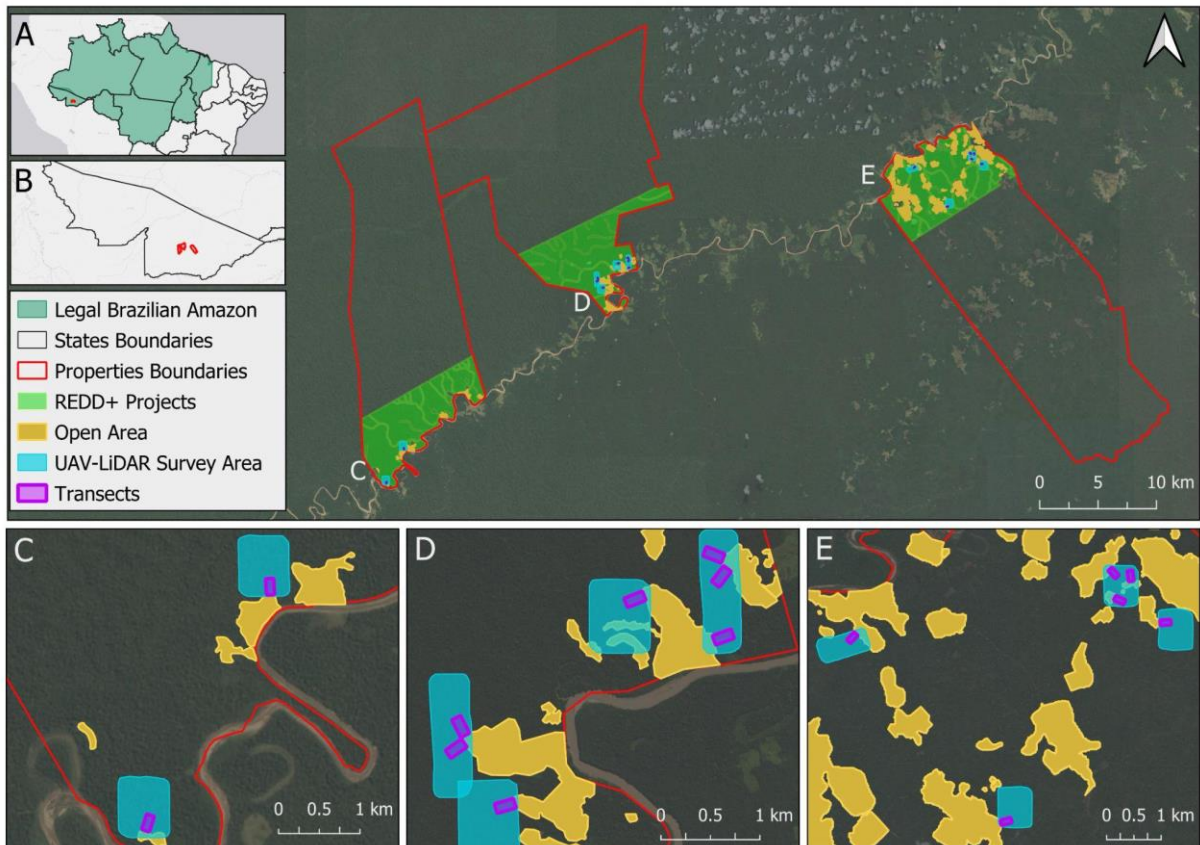


Figure 1. Location map of the study areas; (A) Map of Brazilian Legal Amazon; (B) State of Acre indicating the rural properties; (C, D, E) Detailed maps of each property showing the areas surveyed with UAV-LiDAR and the allocation of sampling transects.

### 3.2.2. LiDAR Data

For LiDAR data collection, we utilized the DJI Zenmuse L1 sensor mounted on the DJI Matrice 300 unmanned aerial vehicle (UAV). The flight planning was conducted using the UgCS Enterprise software, where flight parameters were set at 120 meters altitude with a 70% overlap between collection swaths. The flights were planned to cover areas of forests adjacent to the open areas (Figure 1). For geolocation correction of the data, we employed Post Processed Kinematic (PPK) processing, correcting the latitude, longitude, and altitude using the DJI D-RTK 2 GNSS Mobile Station as the reference base. The point clouds were preprocessed using DJI Terra software. From the point clouds, we generated normalized point clouds and canopy height models (CHM) with a 1-meter resolution using the lidR package (Roussel et al., 2020) in the R software (R Core Team, 2023).

### 3.2.3. Statistical Modelling

We employed statistical modeling to relate the forest's structural attributes to the distance from potential degradation sources (open areas/pastures). To accomplish this, we

mapped the open areas using Planet images and generated a raster that calculated the distance from each pixel to the nearest anthropized area. From the CHM, we generated 10-meter resolution raster layers related to the forest canopy's structural characteristics, including: Canopy Height, Canopy Roughness, Canopy Openness and Carbon Stock. The Canopy Height layer was calculated as the average height within a 10-square-meter area (10x10 grid cells), the Roughness layer was derived from the coefficient of variation of heights, the Openness layer represented the proportion of grid cells below 5 meters in height as a percentage, and the Carbon Stock layer was generated from Canopy Height layer using the equation by Longo et al. (2016) and validated through field inventories within the REDD+ project areas. Additionally, using the normalized point clouds and the LeafR package (Almeida et al., 2021), we generated Leaf Area Index (LAI) and Understory Leaf Area Index layers, with the latter representing the leaf area index below 5 meters in height.

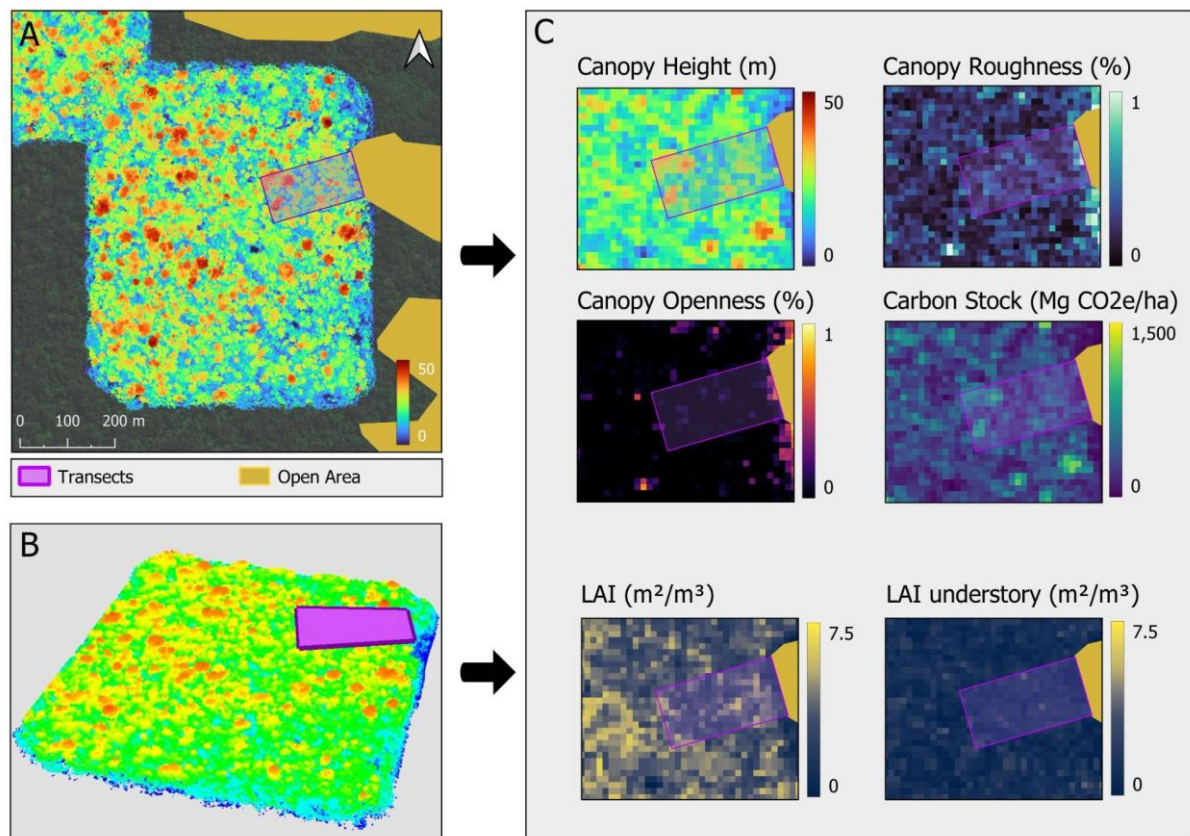


Figure 2. Representation of the structural attributes used in the statistical modeling (C), generated from the Canopy Height Models (CHM) (A), and from the 3D point cloud (B).

We allocated 15 sampling polygons in the form of transects (100m x 200m) in the areas covered by UAV surveys in order to capture the distance gradient starting from the open areas. Next, we used the asymptotic exponential model (Equation 1) to relate the structural attributes with the distance. We chose this model structure to identify the distance at which it

stabilizes, indicating the level of infiltration of the edge effect on the forest structure. We estimated the models for each transect with transect-specific random effects using the JAGS ("Just Another Gibbs Sampler") program through the "jagsUI" package in the software R (Kellner, 2015).

Equation 1. Model used to relate the structural attributes and the distance from the open area.

$$Atr_{gridcell} = \alpha + (\beta - \alpha) * \exp\left(\frac{-dist_{gridcell}}{\gamma}\right)$$

Where:

$Atr_{gridcell}$  = Structural attribute of each grid cell;

$dist_{gridcell}$  = Distance of each grid cell from the open area, m;

The parameters  $\alpha$  (alpha),  $\beta$  (beta), and  $\gamma$  (gamma) in the model allow us to directly interpret the structural condition of the forest. Alpha ( $\alpha$ ) represents the asymptote of the model, indicating the attribute value inside the forest. Beta ( $\beta$ ) is the intercept of the model, representing the attribute value at the forest edge. Gamma ( $\gamma$ ) is the factor related to the rate of change of the attribute value as one moves into the forest. After generating the models for each transect, we estimated an overall model for each attribute, generating a graph with a vertical line indicating the point where the model curve stabilizes.

### 3.3. Results

#### 3.3.1. Statistical modelling

The modeling of structural attributes allowed us to analyze the conditions at the forest edge compared to its interior, as well as indicate how far the edge effect infiltrates into the forest. After generating a model for each attribute for each transect (Figures S1 to S6), we created an overall model for each attribute, where the values of their coefficients alpha ( $\alpha$ ) and beta ( $\beta$ ) represent the average attribute values at forest interior and edge (Figure 4).

For the canopy height attribute, we observed low values at the forest edge, gradually increasing towards the forest interior and reaching an asymptote at 22.8 meters. At the forest edge, the forest height was 9.5 meters, which is 42% lower than the height in the interior. Regarding canopy roughness, we observed an inversely proportional relationship to the distance from the edge. In other words, the roughness decreases as you move further into the forest, with values of 0.23 in the forest interior and 0.64 at the edge, representing a difference

of 41%. For canopy openness, we also found an inversely proportional relationship, where we observed a value of 0.02 in the forest interior and 0.38 at the edge, representing a decrease of 36%. Regarding carbon stock, we observed that the stock at the forest edge is considerably lower compared to the interior, with values of 434.8 Mg CO<sub>2</sub>e/ha in the interior and 110.6 Mg CO<sub>2</sub>e/ha at the edge, representing a 25% lower stock. As for the attributes derived from the point clouds, the leaf area index showed an increasing trend as you move away from the edge, with values of 4.85 m<sup>2</sup>/m<sup>3</sup> in the interior and 2.32 m<sup>2</sup>/m<sup>3</sup> at the edge, representing a difference of 47%. On the other hand, the Understory Leaf Area Index did not show a significant difference between the interior and the edge, with values of 1.7 m<sup>2</sup>/m<sup>3</sup> and 1.19 m<sup>2</sup>/m<sup>3</sup> respectively, indicating consistent values throughout the distance gradient.

We drew an orange dashed line to indicate the point at which the curve of the models stabilizes. In other words, this line represents the level of infiltration of degradation caused by the anthropogenic areas under the forest structure. In our case, as we did not find evidence of selective logging, severe droughts, or wildfires, we consider that this degradation is caused exclusively by the edge effect. By observing the curves of the structural attributes, we can note that Canopy Height and Openness exhibited less infiltration of the edge effect, ranging between 20 and 30 meters. Whereas Canopy Roughness, Carbon Stock and LAI presented higher values, with their model curves stabilizing around 50 meters. LAI understory showed a distinct behavior with consistent values along the distance gradient, suggesting limited influence from the edge effect.

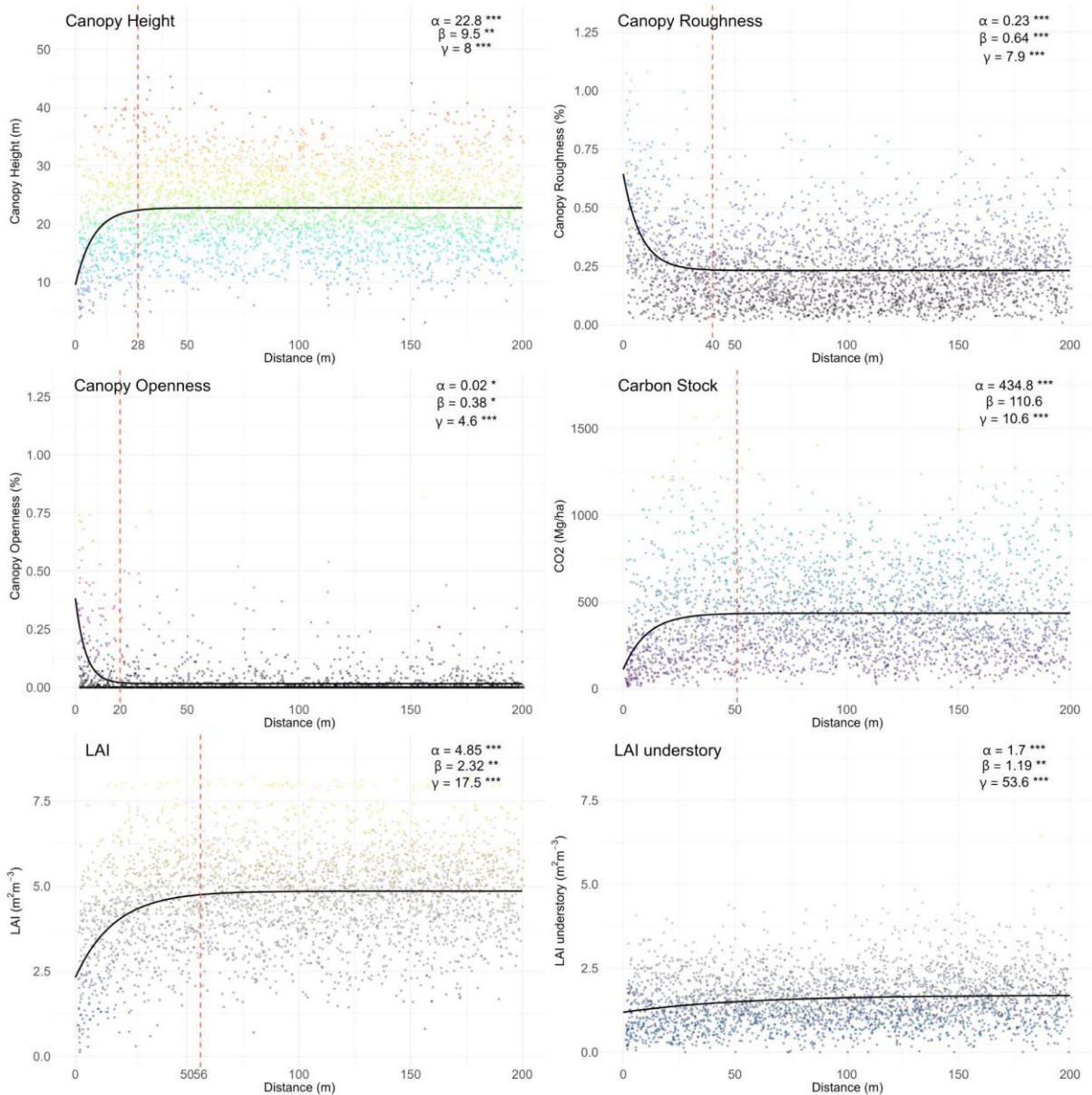


Figure 4. Overall model curves representing the relationship between forest structural characteristics and the distance from open areas. The points on the graph represent the values of the grid cells from all transects. The orange dashed line indicates the distance at which the model curve stabilizes, suggesting the infiltration level of the edge effect into the forest.

### 3.4. Discussion

Our results showed that anthropized areas had a subtle effect on the nearby forests, indicating a low level of degradation in the REDD+ project areas. Although subtle, the methodologies used in this work were able to identify this effect, highlighting the great potential of LiDAR technology for local degradation monitoring. By leveraging the capabilities of LiDAR data, REDD+ projects can improve their ability to identify specific degradation sources, monitor them over time, and estimate associated emissions more

accurately. This information is vital for effective management and conservation strategies, as well as for reporting and verification purposes within the framework of REDD+.

### *Identifying Different Sources of Degradation on REDD+ Projects*

Assessing all potential sources of degradation is crucial for the success of forest conservation in REDD+ projects. By understanding the specific dynamics and potential disturbances in the forest structure, we can develop targeted management approaches to preserve the forest ecosystem and mitigate any potential threats. However, forest monitoring still relies mainly on fieldwork and satellite imagery, which substantially limits its effectiveness. In this study, the use of LiDAR data provided several advantages over satellite-based monitoring systems, enabling a more detailed and efficient assessment of forest structure. Compared to transect walking methodology suggested by VERRA to measure emission from selective logging and illegal timber, the use of UAV-LiDAR system enabled us to cover a larger area of the project, expanding from a few tens to hundreds of hectares of monitored forest. Additionally, it provided inaccessible information in field surveys. Therefore, this methodology also allowed us to assess not only selective logging but also overall forest degradation by accessing the forest structure in detail. Moreover, by employing this methodology, it becomes possible to conduct periodic forest monitoring in REDD+ projects, where identifying discrepancies in forest behavior at a given time can indicate some source of degradation or even the forest's recovery from a degradation event.

Our results showed no signs of selective logging in the project areas. Several studies have highlighted how this activity can alter forest structure (Asner et al., 2006; Dalagnol et al., 2019; Rangel Pinagé et al., 2019; d'Oliveira et al., 2021). In our study, since our results indicate that structural changes in the forest only occur within the first 50 meters (Figure 4), we can consider the absence of such activity, as we know that selective logging can extent hundreds of meters into the forest. These assumptions align with the field walks conducted in the areas, where no evidence of selective logging or illegal timber was identified. In case of selective logging were identified, subsequent procedures would be necessary, such as field visits for validation, estimation of the affected area, and estimation of its emissions.

Additionally, the statistical modeling approach proved to be highly efficient in identifying the presence of the edge effect and assessing its intensity. Evaluating the edge effect is crucial for understanding the level of forest conservation and the effectiveness of the REDD+ project in reducing emissions from degradation. The methodology used allowed us to assess how and to what extent the edge effect alters the forest structure in the project areas,

where UAV-LiDAR data provided detailed information on forest structure. Once the edge effect and its impact on carbon stocks have been identified, future procedures should be implemented to measure the extent of the REDD+ project area affected by the edge effect and estimate its emissions. This information is essential for accurate accounting of emissions and for designing targeted interventions to mitigate the edge effect and enhance the success of the REDD+ project in reducing emissions from forest degradation.

### *Effects of Anthropized Areas on Forest Structure*

Assessing the impact of the edge effect on forest structure and its extent of infiltration is crucial for monitoring the level of degradation in REDD+ projects. Here in this study, the approach allowed us to analyze the impacts of anthropized areas on forest structure, by modeling the forest structure as it moves away from the anthropized area.

The utilization of the asymptotic exponential model provided valuable insights into the behavior of structural attributes of the forest as they extend further away from anthropized areas. Through the analysis of the models curves on the graphs, we observed that Canopy Height, Carbon Stock, and Leaf Area Index (LAI) demonstrated an increasing trend, indicating that as we moved further into the forest, the canopy became taller and denser. This suggests a progressive development of the forest's vertical structure and increased biomass. In contrast, Canopy Roughness and Openness exhibited a decreasing trend with increasing distance from the edge. This implies that as we penetrated deeper into the forest, the canopy became more homogeneous and closed. The understory Leaf Area Index (LAI understory) did not exhibit a significant change as distance from the edge increased. We believe this behavior can be attributed to the age of the opened area, where immediately after the disturbance, there was a rapid growth of understory plants due to plants regeneration. However, over time, these plants grew and reached heights exceeding 5 meters. A similar phenomenon has also been observed in two studies conducted in the Amazon Forest. Malcom (1994) found a high understory LAI at the forest edge shortly after the disturbance, but years later in the same area, Almeida et al. (2019) found that the densest vegetation was located in the midstory, which supports our findings.

All the behaviors were expected considering the edge effect exerted by open areas on adjacent forests (Broadbent et al., 2008; Aragón et al., 2015; Vepakomma et al., 2018; Blachard et al., 2023). However, it is expected that forests with a high level of conservation can inhibit this effect, preventing degradation from infiltrating with high intensity and over long distances. In this study, the rapid stabilization of the curves within the first 50 meters

expressed the high level of forest conservation, highlighting the buffering effect of the forests in the project. If the distance at which the curve stabilizes exceeds the expected infiltration of the edge effect, further investigations should be conducted to identify the source of degradation. Similar results were obtained by Almeida et al. (2019) when evaluating the edge effect in forest fragments of different sizes using the same modelling approach used here, where the largest fragment (100 ha) reached a stabilization point of the curve at 33 meters from the edge. According to the literature review conducted by Broadbent et al. (2008), several studies have found an edge penetration mean distance of 100 meters. However, it is important to mention the different data sources used in these studies, as the use of field data and/or satellite images with different spatial resolutions, can lead to variations in the results due to their ability to detect and quantify changes in forest structure along the edge gradient. Additionally, the results founded in this literature review showed great variance, highlighting the great edge effects variation and the importance of assessing it locally for each REDD+ project.

The variation in the extent of infiltration and intensity of disturbance caused by the edge effect on forest structure is linked to the forest's physiognomy, conservation level, and local microclimate factors. Although our results showed low infiltration in the study areas, around 50 meters, we believe that in landscapes with high fragmentation and adverse climatic conditions, this effect may be more pronounced due to the forest's limited regenerative capacity. Furthermore, another important factor that affects the intensity of the edge effect is the different land uses adjacent to the forest, such as pastures and various agricultural and forestry crops, as they directly affect the microclimate at the forest edge. These land uses can alter factors such as temperature, humidity, soil conditions, and wind patterns, which in turn impact the microenvironment and ecological processes within the forest edge. (Mesquita et al., 1999; Broadbent et al., 2008; Almeida et al., 2019). Therefore, the wide range of factors that influence the edge effect highlights the importance of assessing it locally for each REDD+ project.

### ***Quantifying Emissions from Degradation on REDD+ Projects***

Quantifying emissions from degradation is a crucial aspect of REDD+ projects on carbon market, as it allows for the accurate estimation of carbon stock on the project area. If ignored, there is a significant possibility that projects may be underestimating their emissions. Additionally, it promotes credibility, transparency and accountability, ensuring that projects embrace to rigorous standards and guidelines. Accounting for emissions from degradation is



essential for ensuring fairness in carbon credit generation, allowing project developers to demonstrate that their actions are effectively reducing emissions from degradation in the stage of measurement, reporting, and verification (MRV). Additionally, quantifying such emissions will penalize projects with low effectiveness in conserving their areas. This incentivizes project developers to implement robust conservation measures and actively monitor and address degradation processes. Projects that can effectively measure and reduce degradation emissions are more likely to attract buyers for their carbon credits, as they demonstrate tangible contributions to emission reduction targets. To ensure the effectiveness and replicability of degradation emission quantification, the development of standardized methodologies is crucial. These methodologies should be able to identify and measure various sources of degradation in different areas consistently. This requires a combination of field-based data collection, remote sensing technologies, and modeling approaches that capture the specific characteristics and drivers of degradation in each project location. By establishing robust and efficient methodologies for quantifying degradation emissions, we can enhance the credibility and integrity of REDD+ projects.

The methodology employed in this study has showcased the immense potential of LiDAR data in achieving this goal by analyzing forest structure in detail and identifying degraded areas. Once the degraded areas are identified, following procedures should be undertaken: measuring the extent of the area affected by degradation, estimating the carbon stock in this areas, estimating the carbon stock in reference areas (conserved area), and comparing these estimates to quantify the emissions resulting from degradation. Future studies should be conducted to develop a definitive methodology that encompasses all necessary aspects and provides standardized guidelines for quantifying emissions from degradation accurately. Such a methodology would greatly contribute to the effectiveness and credibility of REDD+ projects by ensuring consistent and reliable measurement, reporting, and verification (MRV) of emissions reductions.

### **3.5. Conclusion**

This study has revealed the significant potential of LiDAR remote sensing technology for monitoring local degradation in REDD+ projects. The methodology utilized allowed for a comprehensive and detailed assessment of forest structure, offering replicable and periodic monitoring capabilities that enhance its effectiveness. Our findings have demonstrated that the impact of open areas on forest structure extends up to 50 meters, showcasing the remarkable resilience of the forests examined in this study. Additionally, the forests adjacent to open

areas exhibited minimal alterations in their structure compared to the interior, indicating a high level of conservation. These results underscore the importance of further research to fully unlock the potential and promote the widespread adoption of UAV-LiDAR systems in the monitoring of REDD+ projects.

## References

Almeida, D R A, Stark, S. C., Chazdon, R., Nelson, B. W., Cesar, R. G., Meli, P., Gorgens, E. B., Duarte, M. M., Valbuena, R., Moreno, V. S., Mendes, A. F., Amazonas, N., Gonçalves, N. B., Silva, C. A., Schiatti, J., & Brancalion, P. H. S. (2019). The effectiveness of lidar remote sensing for monitoring forest cover attributes and landscape restoration. *Forest Ecology and Management*, 438, 34–43. <https://doi.org/10.1016/j.foreco.2019.02.002>

de Almeida, D., Stark, S., Silva, C., Hamamura, C., & Valbuena, R. (2019). leafR: Calculates the leaf area index (LAD) and other related functions. CRAN. <https://cran.r-project.org/web/packages/leafR/index.html>.

Almeida, Danilo Roberti Alves, Almeyda Zambrano, A. M., Broadbent, E. N., Wendt, A. L., Foster, P., Wilkinson, B. E., Salk, C., Papa, D. de A., Stark, S. C., Valbuena, R., Gorgens, E. B., Silva, C. A., Brancalion, P. H. S., Fagan, M., Meli, P., & Chazdon, R. (2020). Detecting successional changes in tropical forest structure using GatorEye drone-borne lidar. *Biotropica*, 52(6), 1155–1167. <https://doi.org/10.1111/btp.12814>

Almeida, Danilo R A, Stark, S. C., Schiatti, J., Camargo, J. L. C., Amazonas, N. T., Gorgens, E. B., Rosa, D. M., Smith, M. N., Valbuena, R., Saleska, S., Andrade, A., Mesquita, R., Laurance, S. G., Laurance, W. F., Lovejoy, T. E., Broadbent, E. N., Shimabukuro, Y. E., Parker, G. G., Lefsky, M., ... Brancalion, P. H. S. (2019). Persistent effects of fragmentation on tropical rainforest canopy structure after 20 yr of isolation. *Ecological Applications*, 29(6), e01952. <https://doi.org/10.1002/eap.1952>

Aragão, L. E. O. C., Poulter, B., Barlow, J. B., Anderson, L. O., Malhi, Y., Saatchi, S., Phillips, O. L., & Gloor, E. (2014). Environmental change and the carbon balance of Amazonian forests. *Biological Reviews of the Cambridge Philosophical Society*, 89(4), 913–931. <https://doi.org/10.1111/brv.12088>

Aragón, G., Abuja, L., Belinchón, R., & Martínez, I. (2015). Edge type determines the intensity of forest edge effect on epiphytic communities. *European Journal of Forest Research*, 134(3), 443–451. <https://doi.org/10.1007/s10342-015-0863-5>

Asner, G. P., Broadbent, E. N., Oliveira, P. J. C., Keller, M., Knapp, D. E., & Silva, J. N. M. (2006). Condition and fate of logged forests in the Brazilian Amazon. *Proceedings of the National Academy of Sciences of the United States of America*, 103(34), 12947–12950. <https://doi.org/10.1073/pnas.0604093103>

Asner, G. P., Kellner, J. R., Kennedy-Bowdoin, T., Knapp, D. E., Anderson, C., & Martin, R. E. (2013). Forest canopy gap distributions in the southern Peruvian Amazon. *Plos One*, 8(4), e60875. <https://doi.org/10.1371/journal.pone.0060875>

Asner, G. P., Knapp, D. E., Broadbent, E. N., Oliveira, P. J. C., Keller, M., & Silva, J. N. (2005). Selective logging in the Brazilian Amazon. *Science*, 310(5747), 480–482. <https://doi.org/10.1126/science.1118051>

Assis, T. O., de Aguiar, A. P. D., von Randow, C., Melo de Paula Gomes, D., Kury, J. N., Ometto, J. P. H. B., & Nobre, C. A. (2020). CO<sub>2</sub> emissions from forest degradation in Brazilian Amazon. *Environmental Research Letters*, 15(10), 104035. <https://doi.org/10.1088/1748-9326/ab9cfc>

Blanchard, G., Barbier, N., Vieilledent, G., Ibanez, T., Hequet, V., McCoy, S., & Birnbaum, P. (2023). UAV-Lidar reveals that canopy structure mediates the influence of edge effects on forest diversity, function and microclimate. *Journal of Ecology*. <https://doi.org/10.1111/1365-2745.14105>

Broadbent, E., Asner, G., Keller, M., Knapp, D., Oliveira, P., & Silva, J. (2008). Forest fragmentation and edge effects from deforestation and selective logging in the Brazilian Amazon. *Biological Conservation*, 141(7), 1745–1757. <https://doi.org/10.1016/j.biocon.2008.04.024>

Camargo, J. L. C., & Kapos, V. (1995). Complex edge effects on soil moisture and microclimate in central Amazonian forest. *Journal of Tropical Ecology*, 11(2), 205–221. <https://doi.org/10.1017/S026646740000866X>

Cochrane, M. A., & Schulze, M. D. (1999). Fire as a recurrent event in tropical forests of the eastern amazon: effects on forest structure, biomass, and species composition. *Biotropica*, 31(1), 2. <https://doi.org/10.2307/2663955>

de Espindola, G. M., de Aguiar, A. P. D., Pebesma, E., Câmara, G., & Fonseca, L. (2012). Agricultural land use dynamics in the Brazilian Amazon based on remote sensing and census data. *Applied Geography*, 32(2), 240–252. <https://doi.org/10.1016/j.apgeog.2011.04.003>

De Sy, V., Herold, M., Achard, F., Asner, G. P., Held, A., Kellndorfer, J., & Verbesselt, J. (2012). Synergies of multiple remote sensing data sources for REDD+ monitoring. *Current Opinion in Environmental Sustainability*, 4(6), 696–706. <https://doi.org/10.1016/j.cosust.2012.09.013>

Diniz, C. G., Souza, A. A. de A., Santos, D. C., Dias, M. C., Luz, N. C. da, Moraes, D. R. V. de, Maia, J. S. A., Gomes, A. R., Narvaes, I. da S., Valeriano, D. M., Maurano, L. E. P., & Adami, M. (2015). DETER-B: The New Amazon Near Real-Time Deforestation Detection System. *IEEE Journal of Selected Topics in Applied Earth Observations and Remote Sensing*, 8(7), 3619–3628. <https://doi.org/10.1109/JSTARS.2015.2437075>

Ferrari, F., Ferreira, M. P., Almeida, C. A., & Feitosa, R. Q. (2023). Fusing Sentinel-1 and Sentinel-2 Images for Deforestation Detection in the Brazilian Amazon Under Diverse Cloud Conditions. *IEEE Geoscience and Remote Sensing Letters*, 20, 1–5. <https://doi.org/10.1109/LGRS.2023.3242430>

Gao, Y., Skutsch, M., Paneque-Gálvez, J., & Ghilardi, A. (2020). Remote sensing of forest degradation: a review. *Environmental Research Letters*, 15(10), 103001. <https://doi.org/10.1088/1748-9326/abaad7>

Gerwing, J. J. (2002). Degradation of forests through logging and fire in the eastern Brazilian Amazon. *Forest Ecology and Management*, 157(1–3), 131–141. [https://doi.org/10.1016/S0378-1127\(00\)00644-7](https://doi.org/10.1016/S0378-1127(00)00644-7)

Goetz, S. J., Hansen, M., Houghton, R. A., Walker, W., Laporte, N., & Busch, J. (2015). Measurement and monitoring needs, capabilities and potential for addressing reduced emissions from deforestation and forest degradation under REDD+. *Environmental Research Letters*, 10(12), 123001. <https://doi.org/10.1088/1748-9326/10/12/123001>

Haugaasen, T., Barlow, J., & Peres, C. A. (2003). Surface wildfires in central Amazonia: short-term impact on forest structure and carbon loss. *Forest Ecology and Management*, 179(1–3), 321–331. [https://doi.org/10.1016/S0378-1127\(02\)00548-0](https://doi.org/10.1016/S0378-1127(02)00548-0)

Hosonuma, N., Herold, M., De Sy, V., De Fries, R. S., Brockhaus, M., Verchot, L., Angelsen, A., & Romijn, E. (2012). An assessment of deforestation and forest degradation drivers in developing countries. *Environmental Research Letters*, 7(4), 044009. <https://doi.org/10.1088/1748-9326/7/4/044009>

Kellner, K. (2015). jagsUI: a wrapper around rjags to streamline JAGS analyses. R package version, 1(1).

Lapola, D. M., Pinho, P., Barlow, J., Aragão, L. E. O. C., Berenguer, E., Carmenta, R., Liddy, H. M., Seixas, H., Silva, C. V. J., Silva-Junior, C. H. L., Alencar, A. A. C., Anderson, L. O., Armenteras, D., Brovkin, V., Calders, K., Chambers, J., Chini, L., Costa, M. H., Faria, B. L., ... Walker, W. S. (2023). The drivers and impacts of Amazon forest degradation. *Science*, 379(6630), eabp8622. <https://doi.org/10.1126/science.abp8622>

Longo, M., Keller, M., dos-Santos, M. N., Leitold, V., Pinagé, E. R., Baccini, A., Saatchi, S., Nogueira, E. M., Batistella, M., & Morton, D. C. (2016). Aboveground biomass variability across intact and degraded forests in the Brazilian Amazon. *Global Biogeochemical Cycles*, 30(11), 1639–1660. <https://doi.org/10.1002/2016GB005465>

McCracken, S., Brondizio, E., Nelson, D., Moran, E., Siqueira, A., & Rodriguez-Pedraza, C. (1999). Remote Sensing and GIS at Farm Property Level: Demography and Deforestation in the Brazilian Amazon. *Photogrammetric Engineering & Remote Sensing*, 65(11), 1311–1320.

Mertz, O., Müller, D., Sikor, T., Hett, C., Heinemann, A., Castella, J.-C., Lestrelin, G., Ryan, C. M., Reay, D. S., Schmidt-Vogt, D., Danielsen, F., Theilade, I., Noordwijk, M. van, Verchot, L. V., Burgess, N. D., Berry, N. J., Pham, T. T., Messerli, P., Xu, J., ... Sun, and Z. (2012). The forgotten D: challenges of addressing forest degradation in complex mosaic landscapes under REDD+. *Geografisk Tidsskrift-Danish Journal of Geography*, 112(1), 63–76. <https://doi.org/10.1080/00167223.2012.709678>

Mesquita, R. C. G., Delamônica, P., & Laurance, W. F. (1999). Effect of surrounding vegetation on edge-related tree mortality in Amazonian forest fragments. *Biological Conservation*, 91(2–3), 129–134. [https://doi.org/10.1016/S0006-3207\(99\)00086-5](https://doi.org/10.1016/S0006-3207(99)00086-5)

MMA. (2014). Brazil's submission of a forest reference emission level for deforestation in the Amazonia biome for results-based payments for REDD+ under the UNFCCC. MMA.

R Core Team, 2022. R: A language and environment for statistical computing. R Foundation for Statistical Computing. URL <https://www.R-project.org/>.

Rangel Pinagé, E., Keller, M., Duffy, P., Longo, M., dos-Santos, M., & Morton, D. (2019). Long-Term Impacts of Selective Logging on Amazon Forest Dynamics from Multi-Temporal Airborne LiDAR. *Remote Sensing*, 11(6), 709. <https://doi.org/10.3390/rs11060709>

Rappaport, D. I., Morton, D. C., Longo, M., Keller, M., Dubayah, R., & dos-Santos, M. N. (2018). Quantifying long-term changes in carbon stocks and forest structure from Amazon forest degradation. *Environmental Research Letters*, 13(6), 065013. <https://doi.org/10.1088/1748-9326/aac331>

Roussel, J.-R., Auty, D., Coops, N. C., Tompalski, P., Goodbody, T. R. H., Meador, A. S., Bourdon, J.-F., de Boissieu, F., & Achim, A. (2020). lidR: An R package for analysis of Airborne Laser Scanning (ALS) data. *Remote Sensing of Environment*, 251, 112061. <https://doi.org/10.1016/j.rse.2020.112061>

Silva, Carlos Alberto, Valbuena, R., Pinagé, E. R., Mohan, M., de Almeida, D. R. A., Broadbent, E. N., Jaafar, W. S. W. M., de Almeida Papa, D., Cardil, A., & Klauberg, C. (2019). ForestGapR: An R Package for Forest Gap Analysis from Canopy Height Models. *Methods in Ecology and Evolution*. <https://doi.org/10.1111/2041-210X.13211>

Silva, Claudia Arantes, Guerrisi, G., Del Frate, F., & Sano, E. E. (2022). Near-real time deforestation detection in the Brazilian Amazon with Sentinel-1 and neural networks. *European Journal of Remote Sensing*, 55(1), 129–149. <https://doi.org/10.1080/22797254.2021.2025154>

Silva Junior, C. H. L., Carvalho, N. S., Pessôa, A. C. M., Reis, J. B. C., Pontes-Lopes, A., Doblaz, J., Heinrich, V., Campanharo, W., Alencar, A., Silva, C., Lapola, D. M., Armenteras, D., Matricardi, E. A. T., Berenguer, E., Cassol, H., Numata, I., House, J., Ferreira, J., Barlow, J., ... Aragão, L. E. O. C. (2021). Amazonian forest degradation must be incorporated into the COP26 agenda. *Nature Geoscience*, 14(9), 634–635. <https://doi.org/10.1038/s41561-021-00823-z>

Thompson, I. D., Guariguata, M. R., Okabe, K., Bahamondez, C., Nasi, R., Heymell, V., & Sabogal, C. (2013). An Operational Framework for Defining and Monitoring ForestDegradation. *Ecology and Society*, 18(2).

UNFCCC. (2014). Report of the technical assessment of the proposed forest reference emission level of Brazil submitted in 2014. UNFCCC.

VCS. (2020). VMD0015 Methods for monitoring of GHG emissions and removals in REDD and CIW projects. VCS.

Wuyts, K., De Schrijver, A., Staelens, J., Gielis, L., Vandenbruwane, J., & Verheyen, K. (2008). Comparison of forest edge effects on throughfall deposition in different forest types. *Environmental Pollution*, 156(3), 854–861. <https://doi.org/10.1016/j.envpol.2008.05.018>

Yang, Y., Saatchi, S. S., Xu, L., Yu, Y., Choi, S., Phillips, N., Kennedy, R., Keller, M., Knyazikhin, Y., & Myneni, R. B. (2018). Post-drought decline of the Amazon carbon sink. *Nature Communications*, 9(1), 3172. <https://doi.org/10.1038/s41467-018-05668-6>

### Supplementary Material

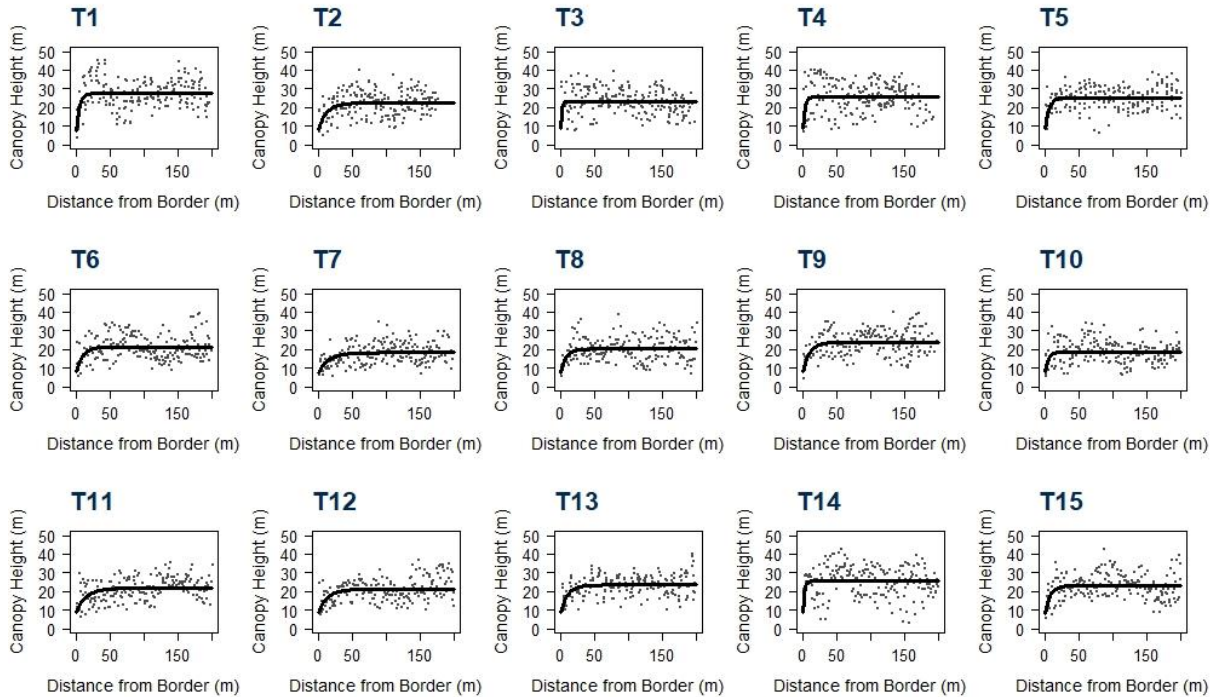


Figure S1. Model of each transect relating distance to canopy height.

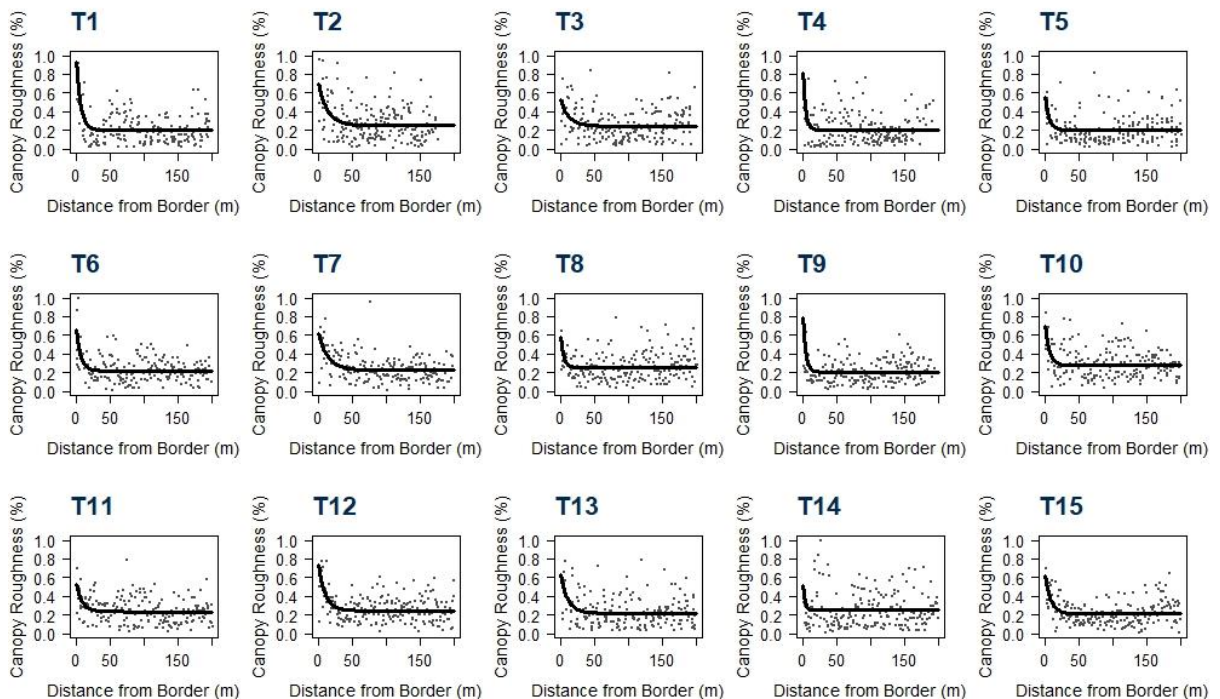


Figure S2. Model of each transect relating distance to canopy roughness.

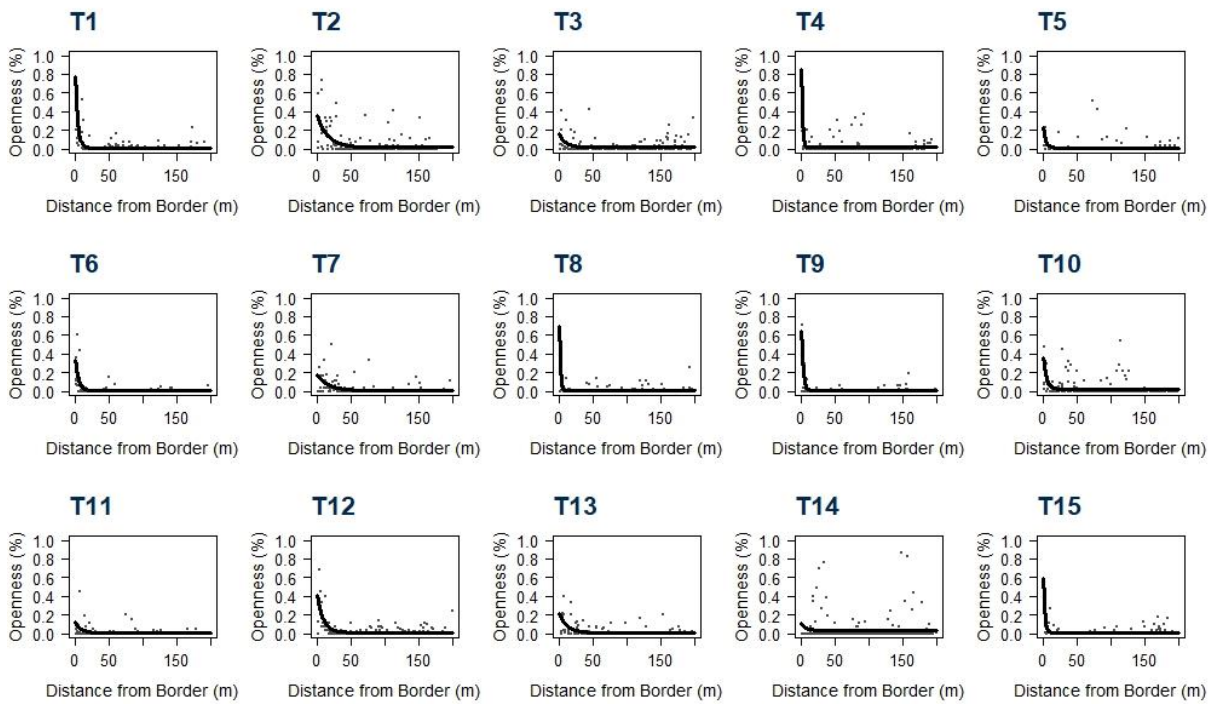


Figure S3. Model of each transect relating distance to canopy openness.

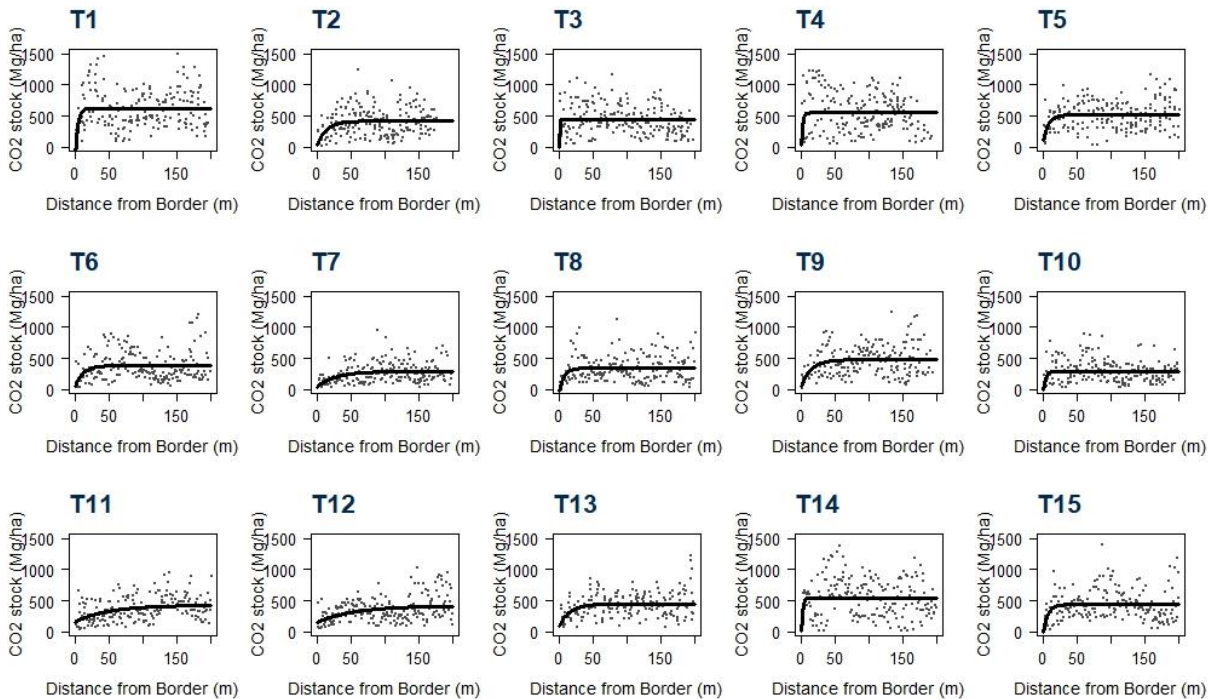


Figure S4. Model of each transect relating distance to carbon stock.

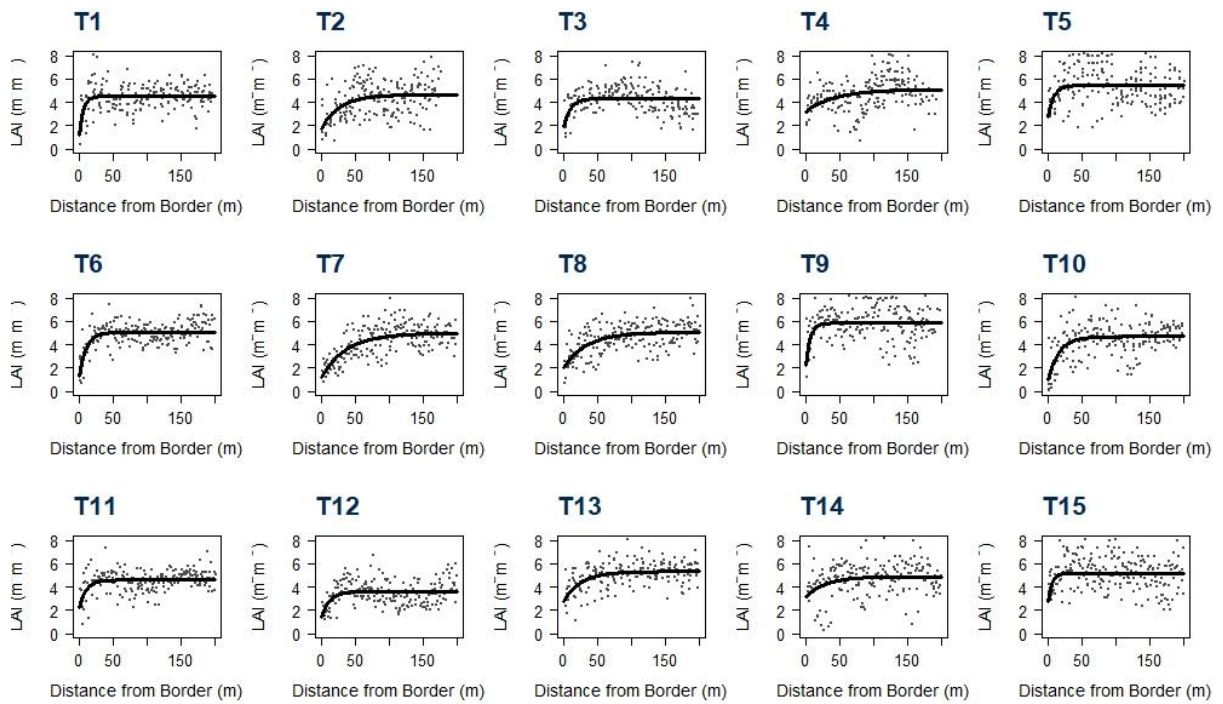


Figure S5. Model of each transect relating distance to leaf area index.

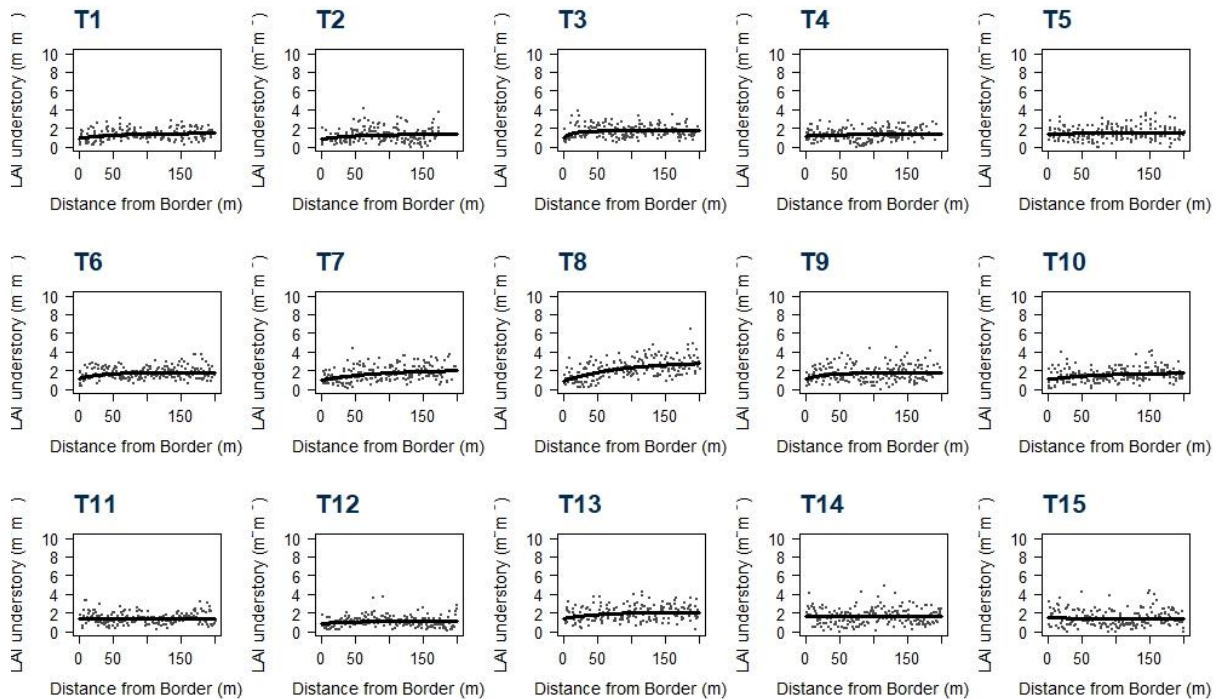


Figure S6. Model of each transect relating distance to leaf area index of the understory.





## 4. FINAL CONSIDERATIONS

In this master's dissertation, we investigate how different remote sensing technologies can enhance forest monitoring programs, increasing their scale and effectiveness without requiring extensive field access. The different forms of remote sensing (passive and active) have their advantages and disadvantages according to their characteristics, and consequently, each one has its best applications. Here, we evaluate different applications of remote sensing for forest monitoring using two different sources of data.

In the first chapter we use passive sensor multispectral satellite imagery to monitor and classify land use of different tree cover classes. The large coverage area of satellite images and their ability to access the spectral behavior in detail, together with the use machine learning algorithm, allowed us to accurately distinguish and locate the different tree cover classes. We aimed at evaluating the potential of high spatial and finer spectral resolution multispectral images from the VEN $\mu$ S satellite to perform supervised classification of contrasted tree cover classes, using the RF machine learning algorithm. To do so, tree cover class characterization was based on their spectral behavior and diversity, generating vegetation indices, delta layers, textural layers, and spectral diversity layers. We obtained high accuracy values (91.9%) and “F1 score” for all classes, which variables were most important for the accuracy of the classification, and finally a description of eventual confusion between tree cover classes. Our study showed that the combination of high spatial and finer spectral resolution multispectral images, different data manipulation techniques, and machine learning algorithms have great potential to assist the classification of tree cover classes across restored forest landscapes, which is expected to be the first step towards the assessment of biodiversity and ecosystem functions. Once the main tree cover classes of a FLR program are identified, further remote sensing approaches, like Lidar technology, and in-deep field assessments can be performed to advance evaluation of FLR benefits for nature and people. Ultimately, the fusion of all these types of data, together with the use of innovative approaches to data processing, can result in novel ways to assess restoration performance and open new avenues to upscale monitoring, bridging the gap between FLR expectations and achieved goals.

In the second chapter, we used LiDAR data (active sensor) along with statistical modeling techniques to access the structural characteristics of the forest and understand the impacts of occupation/opening of areas in REDD+ projects. The ability of this active sensor to access the forest structure allowed us to characterize the condition of the forest and its level

of degradation after a disturbance event, enhancing forest monitoring in REDD+ projects. This study has revealed the significant potential of LiDAR remote sensing technology for monitoring local degradation in REDD+ projects. The methodology utilized allowed for a comprehensive and detailed assessment of forest structure, offering replicable and periodic monitoring capabilities that enhance its effectiveness. Our findings have demonstrated that the impact of open areas on forest structure extends up to 50 meters, showcasing the remarkable resilience of the forests examined in this study. Additionally, the forests adjacent to open areas exhibited minimal alterations in their structure compared to the interior, indicating a high level of conservation. These results underscore the importance of further research to fully unlock the potential and promote the widespread adoption of UAV-LiDAR systems in the monitoring of REDD+ projects.

Finally, the two chapters of this master's dissertation showed practical examples of how remote sensing technologies are key elements for the success of forest monitoring programs. With advanced techniques of data analysis and statistical modelling we can access valuable information about forest characteristics and status. For next steps, robust algorithms need to be developed to automatize the process of data processing and analysis, and standards procedures have to be created to scale up forest monitoring activities, with a combination of satellite imagery, drone surveying and field assessments.